nature materials

Article

https://doi.org/10.1038/s41563-024-01808-0

Immunoengineering can overcome the glycocalyx armour of cancer cells

Received: 21 April 2022

Accepted: 3 January 2024

Published online: 15 February 2024

Check for updates

Sangwoo Park[1,2], Marshall J. Colville[1,2], Justin H. Paek[3], Carolyn R. Shurer[2], Arun Singh[4], Erica J. Secor[5], Cooper J. Sailer[6], Ling-Ting Huang[2], Joe Chin-Hun Kuo[2], Marc C. Goudge[3], Jin Su[5], Minsoo Kim[7], Matthew P. DeLisa[2], Sriram Neelamegham[4], Jan Lammerding[3,8], Warren R. Zipfel[1,3], Claudia Fischbach[3], Heidi L. Reesink[5] & Matthew J. Paszek[1,2,3]

Cancer cell glycocalyx is a major line of defence against immune surveillance. However, how specific physical properties of the glycocalyx are regulated on a molecular level, contribute to immune evasion and may be overcome through immunoengineering must be resolved. Here we report how cancer-associated mucins and their glycosylation contribute to the nanoscale material thickness of the glycocalyx and consequently modulate the functional interactions with cytotoxic immune cells. Natural-killer-cell-mediated cytotoxicity is inversely correlated with the glycocalyx thickness of the target cells. Changes in glycocalyx thickness of approximately 10 nm can alter the susceptibility to immune cell attack. Enhanced stimulation of natural killer and T cells through equipment with chimeric antigen receptors can improve the cytotoxicity against mucin-bearing target cells. Alternatively, cytotoxicity can be enhanced through engineering effector cells to display glycocalyx-editing enzymes, including mucinases and sialidases. Together, our results motivate the development of immunoengineering strategies that overcome the glycocalyx armour of cancer cells.

Clinical interest in cytotoxic immune cells for adoptive cell therapy has swiftly risen due to their ability to kill cells bearing markers associated with oncogenic transformation[1]. Cytotoxic T, natural killer (NK) and NK T cells have been equipped with chimeric antigen receptors (CARs) to direct attacks against cancer cells displaying specific antigens, with a rapidly growing number of therapeutics now in human clinical trials[1–3]. As one barrier to progress, tumour cells can construct a glycocalyx with physical and biochemical attributes that guard against attack by surveilling immune cells and engineered cell therapies[4,5]. Through the stimulation of immunomodulatory receptors, glycans can reprogram the activities of important immune cell types, including macrophages, dendritic cells, cytotoxic T cells and NK cells[6,7]. Larger macromolecules in the cancer cell glycocalyx are also proposed to sterically shield molecular epitopes, fundamentally changing how immune cells perceive and interact with tumour cells[4,8]. Although a multifaceted role for the cancer-associated glycocalyx in immune evasion has become clear, a physical understanding of the glycocalyx remains limited, especially regarding cancer immunotherapy.

In many cancers, disease aggression and poor patient prognosis correlate with enhanced expression of transmembrane mucins, a family

[1]Field of Biophysics, Cornell University, Ithaca, NY, USA. [2]Robert Frederick Smith School of Chemical and Biomolecular Engineering, Cornell University, Ithaca, NY, USA. [3]Nancy E. and Peter C. Meinig School of Biomedical Engineering, Cornell University, Ithaca, NY, USA. [4]State University of New York, Buffalo, NY, USA. [5]Department of Clinical Sciences, College of Veterinary Medicine, Cornell University, Ithaca, NY, USA. [6]Department of Pathology, University of Rochester Medical Center, Rochester, NY, USA. [7]Department of Microbiology and Immunology, David H. Smith Center for Vaccine Biology and Immunology, University of Rochester Medical Center, Rochester, NY, USA. [8]Weill Institute for Cell and Molecular Biology, Cornell University, Ithaca, NY, USA. e-mail: mjp31@cornell.edu

https://doi.org/10.1038/s41563-024-01808-0

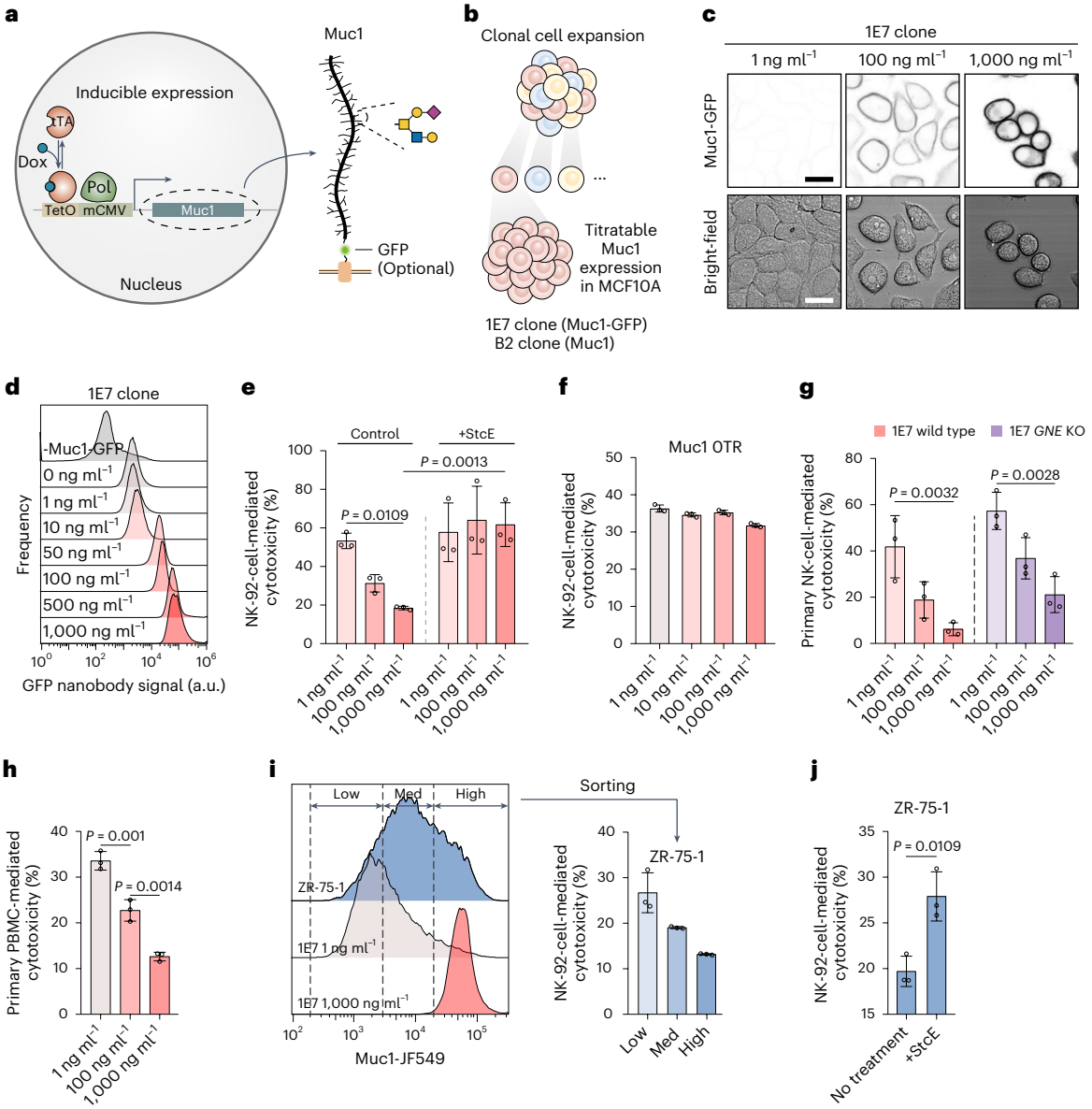

Fig. 1 | Muc1-mediated protection against NK cells. a, Doxycycline (DOX)-inducible system for the controlled expression of Muc1 or Muc1-GFP possessing 42 TRs in MCF10A epithelial cells. **b**, Isolation of stable cell clones with a titratable expression of Muc1-GFP (1E7 clone) or Muc1 (B2 clone). **c**, Fluorescence and bright-field images of 1E7 cells induced at the indicated concentration of doxycycline. Scale bars, 10 µm. **d**, Flow cytometry analysis of 1E7 cells showing titratable Muc1-GFP levels across the indicated concentrations of doxycycline inducer. **e**, NK-92-cell-mediated cytotoxicity against 1E7 cells treated with a control buffer or 100 nM StcE mucinase for 1 h before co-culture; Muc1-GFP induction is at the indicated doxycycline concentration. Results are mean ± standard deviation (s.d.) of $n = 3$ independent experimental replicates. **f**, NK-92-cell-mediated cytotoxicity against an MCF10A cell line expressing a Muc1-GFP construct with the TRs deleted (Muc1 0TR) under the control of a tetracycline-inducible promoter at the indicated doxycycline induction level. Results are mean ± s.d of $n = 3$ technical replicates. **g**, Primary human NK-cell-mediated cytotoxicity against 1E7 cells and 1E7 *GNE* KO cells at the indicated doxycycline concentration. NK-cell-to-target-cell ratio is 5:1. Results are mean ± s.d. of $n = 3$ biological replicates corresponding to three distinct human blood cell donors. **h**, Primary equine PBMC-mediated cytotoxicity against 1E7 cells at the indicated concentration of doxycycline. NK-cell-to-target-cell ratio is 20:1. Results are mean ± s.d. of $n = 3$ biological replicates corresponding to unique equine blood donors. **i**, NK-92-cell-mediated cytotoxicity against ZR-75-1 breast cancer cells sorted into sub-populations with low, intermediate and high endogenous Muc1 expression. NK-cell-to-target-cell ratio is 10:1. Results are mean ± s.d. of $n = 3$ experimental replicates. **j**, NK-92-cell-mediated cytotoxicity against ZR-75-1 treated with a control buffer or 100 nM StcE before co-culture. NK-cell-to-target-cell ratio is 10:1. Results are mean ± s.d. of $n = 3$ independent experimental replicates. Statistical analysis is performed by two-tailed *t*-tests. In **e**, **g** and **h**, statistical analysis is performed by one-way analysis of variance (ANOVA) with Tukey's post hoc tests.

of membrane-anchored biopolymers that are defined by their extensive grafting with O-glycans along an unstructured polypeptide backbone[9]. At high cell-surface densities, mucins form a thick, brush-like layer that has been proposed to shield cells from immune cell recognition[9–11]. Glycans contribute to the steric, hydrophilic and electrostatic interactions that are expected to control the physical properties of the mucin brush and, potentially, immune cell interactions[12,13]. For instance, the truncation of mucin-type O-glycans has been reported to increase NK-cell-mediated cytotoxicity, whereas the elongation of O-glycans has been reported to protect tumour cells[14–17]. However, whether the effects on immune cell resistance are explained by altered glycan–receptor interactions, changes in the structural properties of the glycocalyx or some other consequence of altered glycosylation remains unresolved, in large part, due to challenges associated

with disentangling the biochemical and biophysical effects of altered glycosylation.

Here we combine tools for the precise manipulation and structural measurement of the glycocalyx to demonstrate that the nanoscale thickness of the glycocalyx layer is an important parameter that may explain cellular resistance to NK-92-mediated, CAR NK-92-mediated and CAR T-cell-mediated cytotoxicity. Scanning angle interference microscopy (SAIM) is an optical tool that can measure the glycocalyx thickness with nanometre-scale precision using principles of interferometry[11,18–20]. Taking advantage of an improved implementation of the measurement technology, which we refer to as Ring-SAIM here[21,22], as well as genetic strategies for glycoengineering[23], we resolve how specific molecular features of mucins contribute to the material thickness of the glycocalyx and protect against cytotoxic immune cells. Furthermore, we demonstrate how this protection can be subverted by equipping immune cells with glycocalyx-editing (GE) enzymes to breach the glycocalyx barrier of the target cell.

Densely grafted mucins protect against NK cell attack

The transmembrane mucin, Muc1, is overexpressed in cancers of the breast, pancreas and ovary, as well as many other solid-tumour cancers[24]. To test how cell-surface mucins affect the material thickness of the glycocalyx and immune cell interactions, we developed a cellular model with titratable levels of Muc1. A Muc1-GFP construct with 42 tandem repeats (TRs) of the consensus 20-amino-acid Muc1 repeat and a truncated cytoplasmic tail was stably expressed in MCF10A breast epithelial cells under the control of a tetracycline-inducible promoter (Fig. 1a). The cytoplasmic tail in the Muc1-GFP construct was deleted to limit any potential intracellular signalling that could be induced by Muc1 expression[25]. We isolated several stable MCF10A clonal lines, one referred to as 1E7 here, which exhibited ideal dose responses to doxycycline induction and minimal cell-to-cell variability in Muc1 surface levels (Fig. 1b–d and Extended Data Fig. 1a,b). A similar approach was followed to generate an additional clonal cell line B2 for a titratable expression of the Muc1 construct without the GFP reporter (Fig. 1b and Extended Data Fig. 1c).

We investigated the ability of Muc1 to protect against NK-cell-mediated cytotoxicity initially testing NK-92, a well-characterized NK cell line that is under clinical investigation for use in anticancer cell therapy in humans[26–28]. Increasing the Muc1-GFP expression in 1E7 cells provided progressively stronger protection against killing in NK-92 co-culture assays (Fig. 1e). Similar results were observed for the polyclonal cell line from which the 1E7 clone was isolated, as well as two additional Muc1-GFP-expressing clones and the B2 clonal line expressing Muc1 without the GFP reporter (Extended Data Fig. 1d). A selective removal of the Muc1 ectodomain from 1E7 cells with StcE, a mucin-specific metalloprotease from an enterohemorrhagic *Escherichia coli* strain[29], restored the ability of NK-92 cells to kill the target cells (Fig. 1e and Extended Data Fig. 1e). The genetic deletion of the Muc1 ectodomain similarly abrogated the protection (Fig. 1f). The killing of 1E7 cells by primary human CD56 + NK cells and equine peripheral blood mononuclear cells (PBMCs) also decreased in a dose-dependent manner with increased doxycycline induction of Muc1 in the target cells, suggesting that the protective mechanism mediated by Muc1 may be applicable to broad immune cell populations (Fig. 1g,h and Extended Data Fig. 2a,b).

We benchmarked the Muc1 surface levels in 1E7 cells against ZR-75-1 cells, a breast cancer cell line that is commonly studied as a model of endogenous Muc1 overexpression (OE)[30]. The broad distribution of Muc1 observed in ZR-75-1 cells overlapped with the distributions of Muc1 in 1E7 cells across the full range of doxycycline induction levels (Fig. 1i). NK-92-cell-mediated killing of the cancer cells decreased in a graded fashion with increased endogenous Muc1 surface levels in sorted ZR-75-1 sub-populations (Fig. 1i). The killing of cancer cells was also enhanced following their treatment with StcE (Fig. 1j), verifying that the protection was mediated by the ectodomains of endogenous mucins.

Members of the sialic-acid-binding immunoglobulin-like lectin (Siglec) family of immunomodulatory receptors have been reported to inhibit NK cells in response to ligation with mucin O-glycans and other sialoglycans[31,32]. However, sialoglycans were not strictly necessary for protection by the mucin layer. In line with prior reports[31–33], we found that CD56 + NK-92 cells expressed minimal to no detectable levels of Siglec-7 and Siglec-9—the primary Siglec family members linked to NK cell inhibition (Extended Data Fig. 2a–d). Furthermore, protection by the mucin layer against primary human NK cells was still evident, although somewhat reduced, following the complete ablation of sialylation in target 1E7 cells through the knockout (KO) of the glucosamine (UDP-*N*-acetyl)-2-epimerase/*N*-acetylmannosamine kinase gene *GNE* (Fig. 1g and Extended Data Fig. 2e).

Although mucins might stimulate immunomodulatory receptors other than siglecs, our results were consistent with the alternative possibility that changes in mucin levels or glycosylation patterns could affect the physical structure of the glycocalyx to modulate interactions with cytotoxic immune cells. Indeed, using Ring-SAIM to measure the thickness of the glycocalyx, we observed a large increase in the glycocalyx thickness for the 1E7 model with enhanced mucin expression, corresponding to the greater protection against NK-92 and primary NK cells (Fig. 1e,g and Fig. 2a–c; Supplementary Note 1 provides a complete description of Ring-SAIM). Likewise, the glycocalyx thickness of ZR-75-1 breast cancer cells dramatically decreased from 109 ± 19 to 61 ± 18 nm following the selective removal of mucins with StcE, corresponding to their diminished resistance to killing by NK-92 cells (Figs. 1j and 2d).

Molecular determinants of the protective mucin barrier

To assess whether changes to the physical structure of the glycocalyx might alter susceptibility to cytotoxic immune cell attacks, we sought a better understanding of how specific molecular attributes of

Fig. 2 | Molecular determinants of the protective mucin layer. a, Schematic of Ring-SAIM; interference of direct and reflected laser light off a silicon mirror creates standing waves of excitation light that depend on the laser incidence angle θ and are used to probe the glycocalyx thickness, which is measured as the gap between the substrate and fluorescently labelled membrane. **b**, Optical configuration for Ring-SAIM showing azimuthally scanned excitation light at varying θ. AOTF, acousto-optic tunable filter. **c**, Representative wide-field image and glycocalyx thickness map of live 1E7 cells expressing Muc1-GFP at the indicated doxycycline induction level. Scale bars, 10 µm. **d**, Glycocalyx thickness in ZR-75-1 cells before and after treatment with 100 nM StcE. The boxes and whiskers show the first and third quartiles (boxes), median and range of data. Each condition includes a minimum of six cells from a representative experiment ($n = 3$ independent experiments). Statistical analysis is performed by a two-tailed *t*-test. **e**, Biosynthetic pathway for mucin-type O-glycans. **f**, Relative O-glycan distributions measured by the CORA analysis in 1E7 wild-type, 1E7 *GCNT1* OE, 1E7 *C1GALT1* KO and 1E7 *GNE* KO cells. **g**, Glycocalyx thickness in the 1E7 cell panel at the indicated doxycycline concentration; some cellular treatments include 10 µM recombinant human Gal-1, 5 µM recombinant human Gal-3 or 10 µM TD139. The boxes and whiskers show the first and third quartiles (boxes), median and range of data. Each condition includes a minimum of 13 cells from a representative experiment ($n = 3$ independent experiments). Statistical analysis is performed by one-way ANOVA with Tukey's post hoc tests. **h**, NK-92-cell-mediated cytotoxicity against the wild-type and engineered 1E7 cells at the indicated doxycycline induction level. NK-cell-to-target-cell ratio is 5:1. Results are mean ± s.d. of at least $n = 3$ independent experimental replicates. Statistical analysis is performed by one-way ANOVA with Tukey's post hoc tests. **i**, NK-92-cell-mediated cytotoxicity is inversely proportional to the measured glycocalyx thickness with a Pearson correlation coefficient of $r = -0.91$; plotted data are obtained from **g** and **h**; the dashed line indicates a linear fit to the data.

https://doi.org/10.1038/s41563-024-01808-0

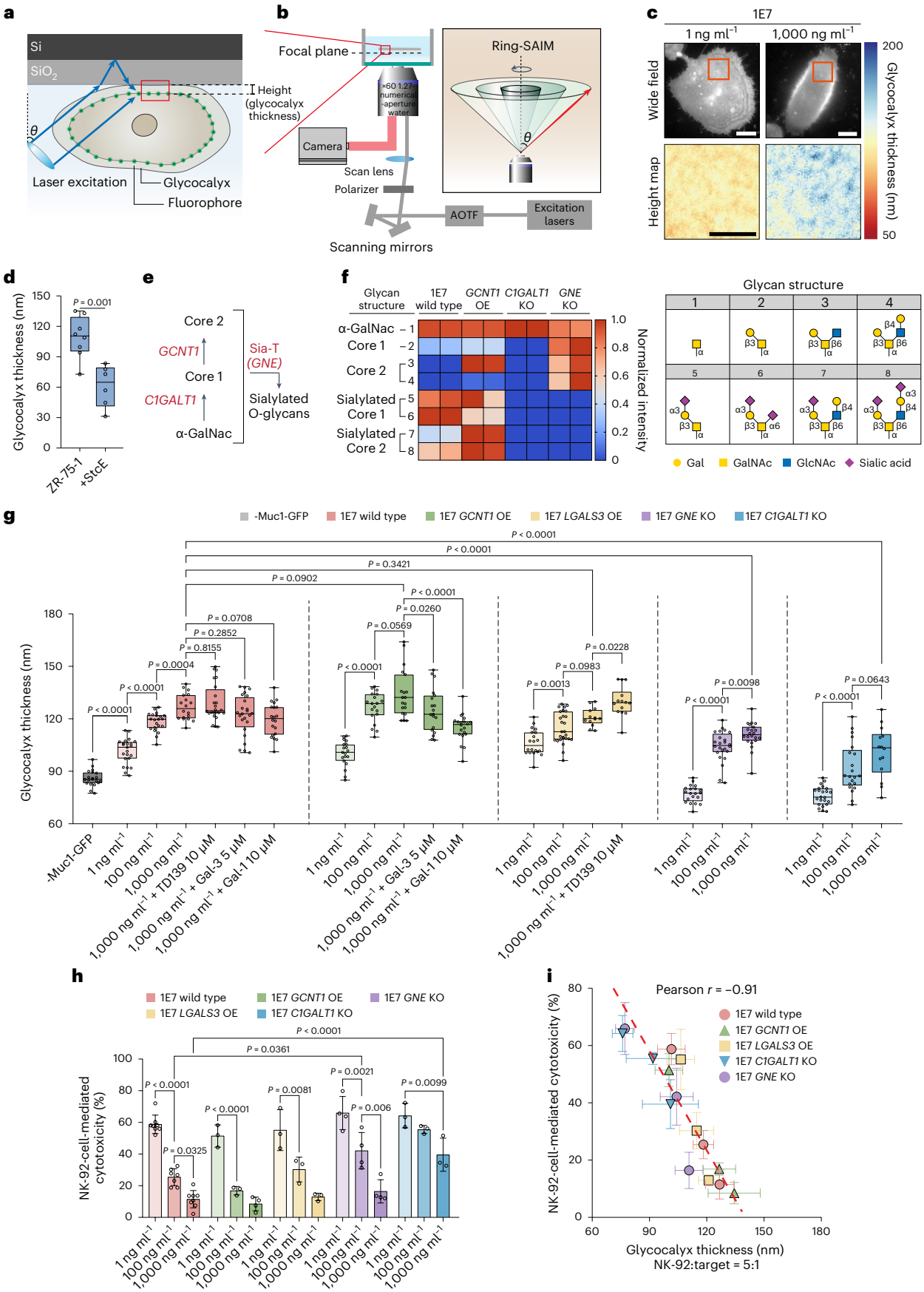

https://doi.org/10.1038/s41563-024-01808-0

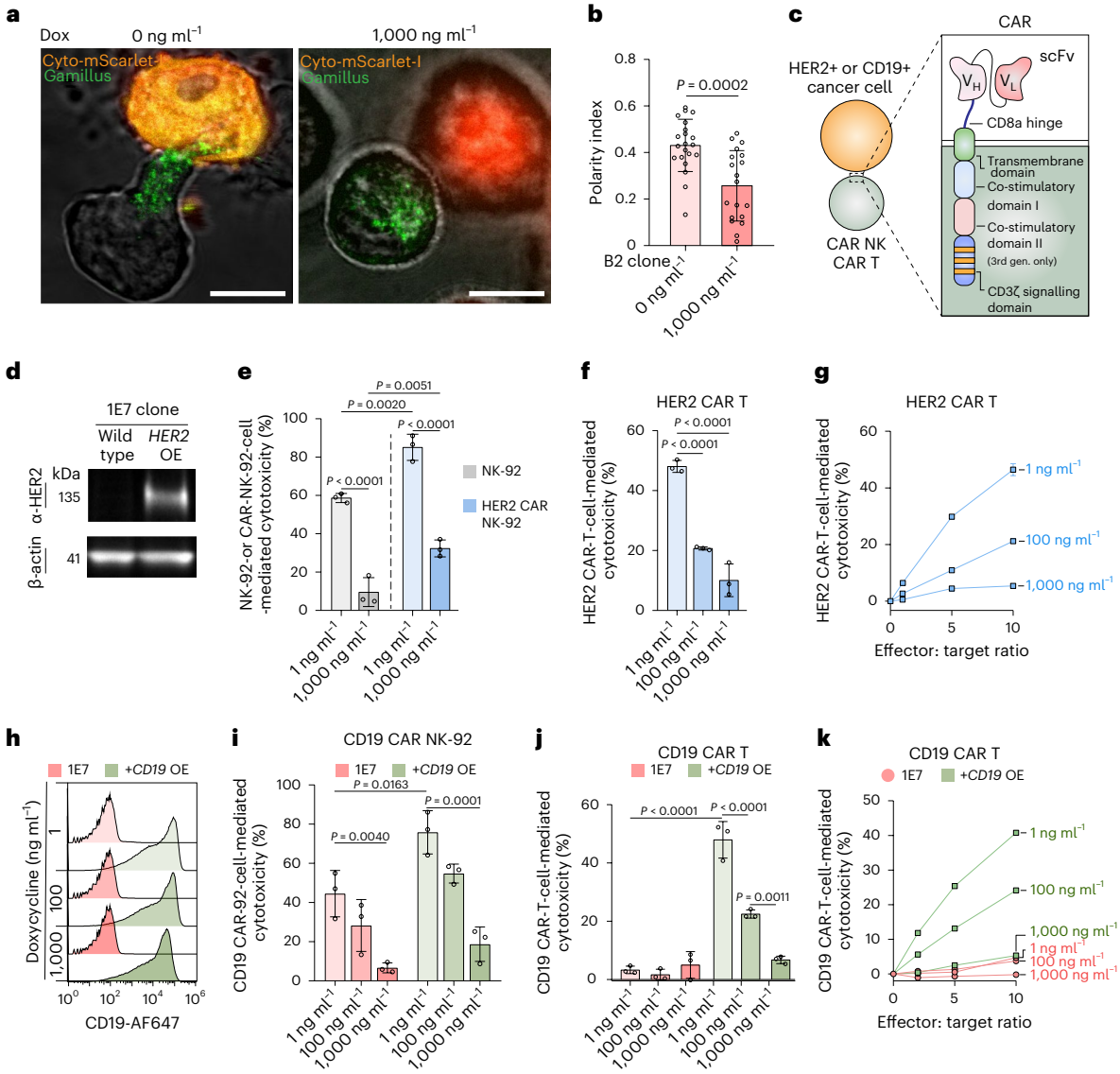

Fig. 3 | Enhanced receptor-mediated activation can overcome the mucin barrier. a, Representative fluorescence images of endogenous GzmB-Gamillus in NK-92 cells following conjugation with Muc1-expressing B2 cells at the minimal and maximal doxycycline induction of Muc1 expression; B2 cells also express cytosolic mScarlet-I as a red fluorescent marker. Scale bars, 10 µm. **b**, Polarity index for Gamillus-labelled cytolytic granules in NK-92 cell conjugates with B2 cells at the indicated doxycycline induction of Muc1 (0 and 1,000 ng ml^{-1}). Results are mean ± s.d. of at least 38 cells over $n = 3$ independent experimental replicates. Statistical analysis is performed by a two-tailed t-test. **c**, Schematic showing the structure of CAR-targeting HER2 and CD19. V_H and V_L are the heavy and light chain variable fragments of the anti-CD19 or anti-HER2 antibody. **d**, Western blot analysis of HER2 in wild-type and HER2-overexpressing 1E7 cells (+HER2 OE). **e**, NK-92 and HER2 CAR NK-92-cell-mediated cytotoxicity against 1E7 *HER2* OE cells at the indicated concentration of doxycycline. **f**, HER2 CAR T-cell-mediated cytotoxicity against 1E7 *HER2* OE cells at the indicated concentration of doxycycline. **g**, HER2 CAR T-cell-mediated cytotoxicity against 1E7 *HER2* OE cells at the indicated doxycycline induction level and target:effector ratio. **h**, Flow cytometry analysis of CD19 surface levels on 1E7 wild-type and *CD19*-overexpressing 1E7 cells (+*CD19* OE) cells at the indicated concentrations of doxycycline. **i**, NK-92 and CD19 CAR NK-92-cell-mediated cytotoxicity against 1E7 or *CD19* OE 1E7 cells at the indicated concentration of doxycycline. $n = 3$ independent experimental replicates. **j**, CD19 CAR T-cell-mediated cytotoxicity against 1E7 and 1E7 *CD19* OE cells at the indicated concentration of doxycycline. **k**, CD19 CAR T-cell-mediated cytotoxicity against 1E7 and 1E7 *CD19* OE cells at the indicated doxycycline induction level and target:effector ratio. Unless otherwise indicated, effector-cell-to-target-cell ratio is 5:1. All the results in **e**–**g** and **i**–**k** are shown as mean ± s.d. of $n = 3$ independent experimental replicates. In **e**, **f**, **i** and **j**, statistical analysis is performed by one-way ANOVA with Tukey's post hoc tests. HER2 CAR NK-92/T and CD19 CAR T cells are second-generation CARs, whereas CD19 CAR NK-92 is a third-generation CAR.

mucins contribute to the ensemble materials properties of the glycocalyx. Noting that the height of a polymer brush is known to scale with the polymer grafting density and polymer chain length with additional contributions from the polymer side chains[34–36], we sought to quantitatively evaluate the effects of mucin surface density, backbone size and glycosylation on the glycocalyx thickness.

We first validated the sensitivity of Ring-SAIM to detect small, nanometre-scale changes in the glycocalyx thickness using Muc1 constructs with varying numbers of TR as size standards (Fig. 2a,b and Extended Data Fig. 3a–f)[21]. We next measured the thickness of the glycocalyx in 1E7 and B2 cells at varying doxycycline induction levels to control the mucin surface levels, observing a progressive increase in glycocalyx thickness with increased Muc1-GFP or Muc1 expression (Fig. 1g and Extended Data Fig. 3g). The glycocalyx thickness scaled with the mucin chain length and surface density, consistent with the expected behaviours of a polymer brush (Extended Data Fig. 3h,i). Mutation of the serine and threonine O-glycosylation sites in Muc1 TRs to alanine dramatically reduced the glycocalyx thickness,

https://doi.org/10.1038/s41563-024-01808-0

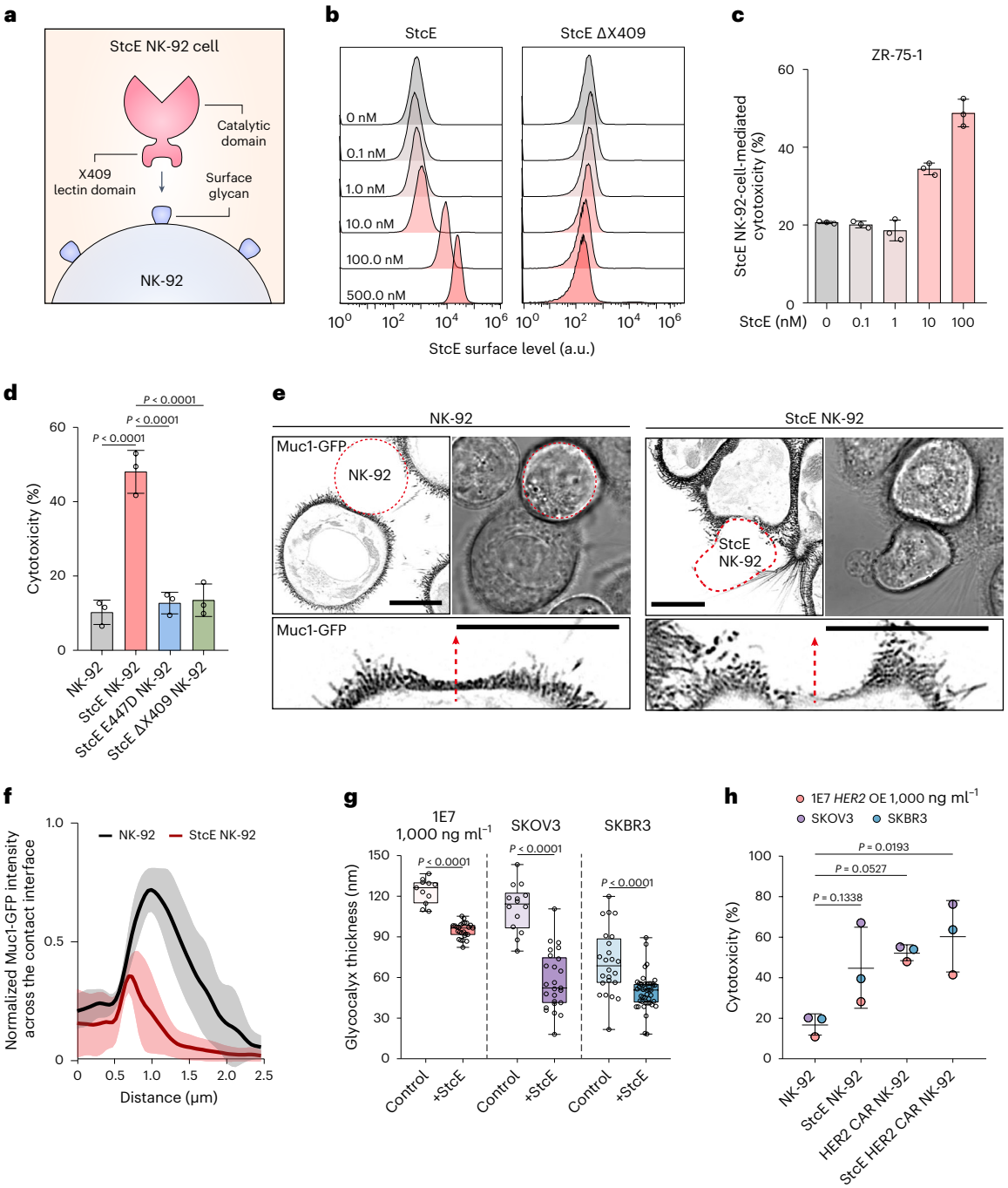

Fig. 4 | Tethering StcE mucinase to the NK-92 cell surface enhances the cytolytic efficiency. a, StcE NK-92 cells prepared through the tethering of StcE mucinase to the NK-92 cell surface by the native StcE X409 lectin domain. **b**, Surface levels of StcE and X409-deleted StcE (StcE ΔX409) on NK-92 cells following mucinase incubation at the indicated concentrations. **c**, ZR-75-1 cell killing by StcE NK-92 cells prepared with the indicated StcE concentration. NK-cell-to-target-cell ratio is 10:1. Results are mean ± s.d. of $n = 3$ technical replicates. **d**, Killing of 1E7 cells by NK-92, StcE NK-92, NK-92 cells tethered with catalytically dead StcE E447D and NK-92 cells treated with StcE ΔX409. NK-cell-to-target-cell ratio is 10:1. Results are mean ± s.d. of $n = 3$ independent experimental replicates. **e**, Bright-field and Muc1-GFP fluorescence images of 1E7 cells conjugated with NK-92 or StcE NK-92 cells; the bottom images show zoomed-in regions of the NK–1E7 cell interface. Scale bars, 10 μm. **f**, Mean Muc1-GFP intensity (dark lines) and s.d. values (lighter bounding areas) along line profiles across the contact interface between 1E7 cell and NK-92 cells ($n = 6$) or StcE NK-92 cells ($n = 10$); the intensity is normalized to the mean intensity outside the contact interface; the red dotted arrows in **e** show the representative profile lines. **g**, Glycocalyx thickness before and after treatment with 100 nM StcE. The boxes and whiskers show the first and third quartiles (boxes), median and range of data. Each condition includes a minimum of 11 cells from a representative experiment ($n = 3$ independent experiments). Statistical analysis is performed by a two-tailed *t*-test. **h**, Cytotoxicity mediated by control and engineered NK-92 cells. Results are mean ± s.d. of $n = 3$ target cancer cell lines with individual data points indicating the average cytotoxicity against a specific cell line (SKOV3, SKBR3 and 1E7 *HER2* OE). NK-cell-to-target-cell ratio is 5:1 for 1E7 *HER2* OE and 10:1 for SKOV3 and SKBR3. In **d** and **h**, statistical analysis is performed by one-way ANOVA with Tukey's post hoc tests. For all the experiments, Muc1-GFP expression in 1E7 and 1E7 HER2 OE cells was with 1,000 ng ml^{-1} doxycycline.

quantitatively demonstrating the additional importance of O-glycan side chains to the brush structure (Extended Data Fig. 3j).

We next investigated how the O-glycan size and charge contribute to the glycocalyx structure by generating glycoengineered progenies of the 1E7 cell model. O-glycans were truncated through the homozygous KO of the *C1GALT1* gene, which encodes Core 1 synthase, the enzyme that catalyses the extension of O-glycans beyond the initiating *N*-acetylgalactosamine (GalNAc) monosaccharide (Fig. 2e and Extended Data Fig. 4a,b). The sizes of O-glycan structures were extended through the OE of *GCNT1* to increase glucosaminyl (*N*-acetyl) transferase 1 (GCNT1), the enzyme that governs Core 2 branching and the subsequent elongation of O-glycans (Fig. 2e and Extended Data Fig. 4c). Negative charges on O-glycans were diminished through the KO of *GNE* to abrogate sialylation (Extended Data Figs. 2e and 4e). The expected glycan alterations were validated with the cellular O-glycome reporter/amplification (CORA) assay, as well as additional biochemical analyses with lectin and antibody probes (Fig. 2f and Extended Data Fig. 4c–g)[37]. The glycoengineered cell lines displayed typical morphologies and normally proliferated only with the *C1GALT1* KO cells, exhibiting a moderate decline in growth rate (Extended Data Fig. 4h).

At each Muc1-GFP induction level, the glycocalyx was significantly thinner in *C1GALT1* and *GNE* KO cells compared with 1E7 cells with wild-type glycosylation (Fig. 2g). We confirmed that at equivalent doxycycline induction concentrations, the wild-type and glycoengineered 1E7 cells had comparable levels of Muc1 on the cell surface (Extended Data Fig. 4i). At full doxycycline induction, the truncation of glycans through *C1GALT1* KO had the largest effect on the glycocalyx, reducing the thickness by approximately 25 nm compared with cells with wild-type O-glycosylation. The KO of *GNE* to ablate sialylation reduced the average glycocalyx thickness by 16.0 nm, whereas *GCNT1* OE to catalyse glycan elongation increased the average glycocalyx thickness by 7.6 nm (Fig. 2g).

Multivalent galectins have been proposed to potentially crosslink and increase the barrier properties of cell-surface mucins[38]. Although we observed the specific interactions of galectin-1 (Gal-1) and galectin-3 (Gal-3) with Muc1 O-glycans, the glycocalyx thickness for 1E7 cells at high Muc1-GFP induction levels did not significantly change following cellular treatment with recombinant human galectin-1 (rhGal-1), recombinant human galectin-3 (rhGal-3) or the small-molecule inhibitor of galectin binding, namely, TD139 (Fig. 2g and Extended Data Fig. 5a–h; TD139, K_d = 0.036 μM for Gal-3). A small but significant increase in the glycocalyx thickness was observed following the TD139 treatment of 1E7 cells that overexpressed *LSGAL3* (Fig. 2g and Extended Data Fig. 4f). The most pronounced effect was observed for *GCTN1* OE 1E7 cells following rhGal-1 and rhGal-3 treatments, which resulted in the compaction of the glycocalyx layer by approximately 19 and 10 nm, respectively (Fig. 2g). The larger effect for Gal-1 was consistent with its strong binding preference for Core 2 O-glycans whose synthesis was governed by GCNT1 (Extended Data Fig. 5g,h). Fluorescence recovery after photobleaching studies confirmed that mucins were mobile in the cell-surface brush and not linked into a more extended, gel-like network, even after Gal-1 treatment (Extended Data Fig. 5i–k). The galectin-mediated contraction of the glycocalyx was consistent with the predicted behaviour of a polymer brush with more self-chain or interchain links[39]. Overall, these results provided a framework for understanding the mucin-rich glycocalyx as a polymer brush whose properties are tuned by glycosylation and, potentially, some crosslinking.

Immune protection correlates with the glycocalyx thickness

Our SAIM measurements and biochemical analyses provided a roadmap for how the material and biochemical states of the glycocalyx could be manipulated by tuning the mucin density and glycosylation. Armed with this information, we next tested how specific glycocalyx states would protect against cytotoxic immune cells. 1E7 cells at varying Muc1-GFP induction levels and their glycoengineered progenies were co-incubated with NK-92 cells to assess the cytotoxicity. Across the glycoengineered panel, NK-92-cell-mediated cytotoxicity against the mucin-expressing target cells was progressively reduced at higher doxycycline induction levels (Fig. 2h). Mucins with truncated and less sialylated O-glycans provided less protection against NK-92 cells (Fig. 2h). Thus, resistance to NK-92-cell-mediated cytotoxicity appeared to correlate with conditions that favoured the extension of a thicker glycocalyx.

To assess the relationship between resistance to immune cell attack and glycocalyx material thickness, the NK-92-cell-mediated cytotoxicity (Fig. 2h) was plotted against the measured glycocalyx thickness (Fig. 2g) for each of the glycoengineered cell types and Muc1-GFP induction levels. We observed a strong and nearly perfect inverse correlation between cytotoxicity and glycocalyx material thickness across the combined dataset representing different mucin expression levels and glycosylation patterns (Fig. 2i). The cytotoxicity data were fit to a linear model dependent on a single variable—the glycocalyx thickness (Pearson coefficient = −0.91; Fig. 2i). Remarkably, we found that the glycocalyx thickness explained approximately 83% of the variance in NK-92-cell-mediated cytotoxicity across the full glycoengineered cell panel, which presents glycocalyces with widely varying glycosylation patterns and biochemical attributes. Although these results did not preclude the stimulation of immunomodulatory receptors as a mechanism of protection by the glycocalyx layer, the biophysical effects associated with mucin OE may have had a predominant role in cellular protection given the strong correlations with glycocalyx thickness.

CARs boost immune cell killing of mucin-protected cells

We investigated in more detail how the glycocalyx layer could protect against immune-cell-mediated cytotoxicity. The direct inhibition of apoptotic pathways was unlikely, since Muc1 expression did not significantly protect the target cells from exogenously applied perforin and apoptotic agents (Extended Data Fig. 6). The live-cell imaging of NK-92 and 1E7 cells also revealed prolonged cell–cell contacts between the effector and high-Muc1-expressing target cells, suggesting a more complex protective role of the Muc1 polymer brush beyond functioning as a simple steric barrier that prevents immune cell conjugation (Fig. 3a).

We considered whether Muc1 might interfere with immune receptor activation or downstream signalling processes that lead to cytolytic granule polarization. Cytolytic granules were labelled through CRISPR/Cas9 knock in of the pH-tolerant green fluorescent protein, Gamillus, at the endogenous *GZMB* locus of NK-92 cells to create a granzyme B (GzmB) fusion protein (Fig. 3a and Extended Data Fig. 7). Even with prolonged cell–cell contact, cytolytic granules often failed to polarize in NK-92 cells conjugated with target cells expressing high levels of Muc1 (Fig. 3a). The polarity index, a quantification of the angular distribution of fluorescent signal from the cytolytic granules with respect to the centre of mass of the immune cell[40,41], decreased by 59.6% in NK-92 cells conjugated with target cells expressing high versus low levels of Muc1 (Fig. 3b).

We noted that if Muc1 interfered with immune receptor activation and signalling, then boosting the stimulatory signalling through immune cell engineering should at least partially override the protection mediated by mucins. To test this, we equipped NK-92 cells and primary human T cells with CARs against human epidermal growth factor receptor-2 (HER2) and CD19 (Fig. 3c–k). As our target cell models, *HER2* or *CD19* were overexpressed in 1E7 cells, which otherwise express low levels of HER2 and no detectable levels of CD19. The mucin layer

https://doi.org/10.1038/s41563-024-01808-0

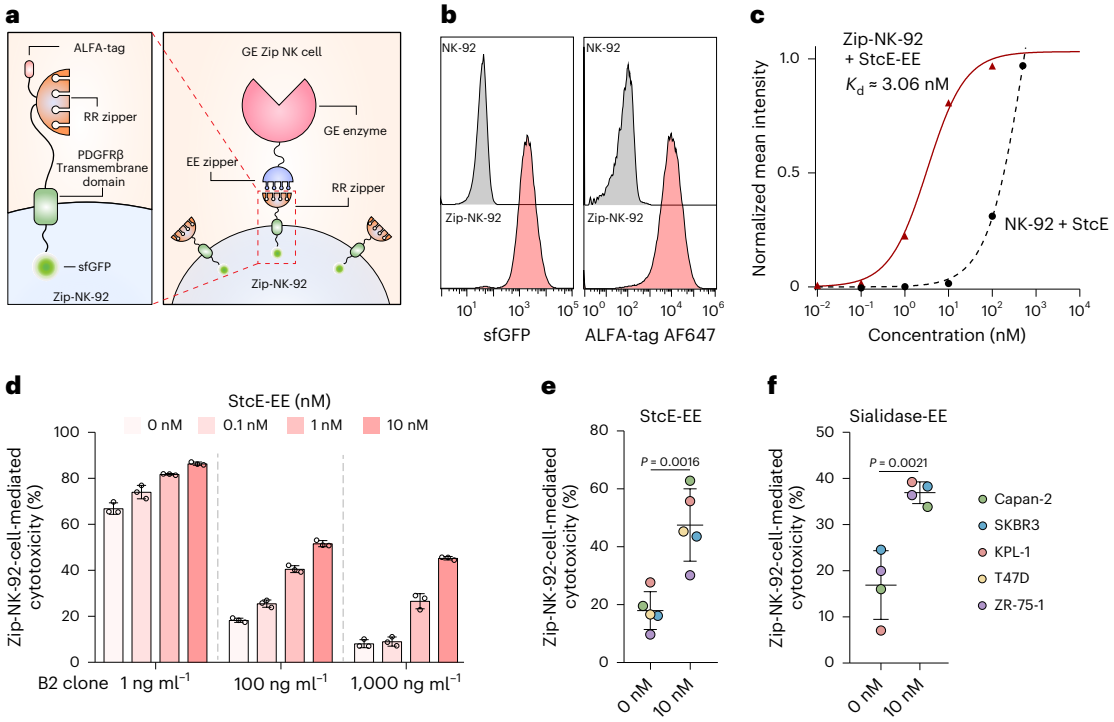

Fig. 5 | Zip-NK-92 cells for the modular display of GE enzymes. a, Cartoon showing the design of Zip-NK-92 cells for the modular surface display of GE enzymes using leucine zippers. **b**, Flow cytometry analysis of sfGFP and ALFA-tag on wild-type NK-92 and Zip-NK-92 cells expressing the membrane-anchored RR zipper. **c**, Binding isotherms for StcE-EE zipper fusion protein (StcE-EE) incubated with Zip-NK-92 cells (red) and wild-type StcE incubated with NK-92 cells (black). Representative normalized intensity plot from $n = 3$ independent experimental replicates. **d**, Cytotoxicity mediated by Zip-NK-92 cells coupled with StcE-EE at the indicated concentration against Muc1-expressing B2 cells at the indicated doxycycline induction level. NK-cell-to-target-cell ratio is 5:1. Results are mean ± s.d. of $n = 3$ technical replicates for each doxycycline level. **e**,**f**, Cytotoxicity mediated by Zip-NK-92 cells coupled with the indicated concentration of StcE-EE (**e**) and sialidase-EE (**f**) against the target cancer cell lines. NK-cell-to-target-cell ratio is 10:1. Results are mean ± s.d. of $n = 4$ or 5 target cancer cell lines (Capan-2, SKBR3, KPL-1, T47D and ZR-75-1). Statistical analysis is performed by a two-tailed t-test.

still provided noticeable protection against CAR-equipped NK-92 and T cells as demonstrated by the ability of increased Muc1-GFP expression in the target cells to progressively defend against killing (Fig. 3e–g,i–k). However, the equipment of NK-92 cells with the HER2 CAR enhanced killing by 3.4-fold against *HER2*-overexpressing 1E7 cells (1E7 *HER2* OE) at high Muc1-GFP induction, indicating that the protection mediated by the glycocalyx layer could be circumvented at least partially through increased receptor-mediated stimulation (Fig. 3e). Likewise, CD19 NK-92 and T cells generally showed higher cytotoxic effects against positive CD19 versus negative 1E7 cells at similar Muc1-GFP induction levels (Fig. 3i–k). We confirmed that Muc1-GFP expression in the target 1E7 cells did not affect the CD19 surface levels, indicating that differences in the total ligand levels probably did not account for the reduced target cell killing (Fig. 3h). Taken together, these results support the use of CARs as a strategy to enhance the killing of mucin-bearing targets.

Surface-displayed mucinases can enhance NK cell killing

We considered alternative engineering strategies that could be independently used or in synergy with CARs to enhance the immune cell killing of target cells that express high levels of mucin. Enterohemorrhagic *E. coli* utilize the StcE mucinase to breach the gut mucosal barrier and adhere to intestinal cells[29]. We reasoned that StcE mucinase might similarly be equipped on the effector immune cell surface to breach the mucin barrier on target cells[42]. Exploring strategies to tether StcE to effector immune cells, we noted that recombinant StcE readily and specifically bound to the NK-92 cell surface, where it was retained for prolonged periods even after stringent washing with a buffer (Fig. 4a,b). StcE ΔX409 with a deleted C-terminal lectin domain was not retained on the NK-92 surface, indicating that the X409 domain was the primary binding module that mediated tethering (Fig. 4b).

Compared with unmodified NK-92 cells, the StcE-equipped NK-92 (StcE NK-92) cells were considerably more effective at killing ZR-75-1 breast cancer cell lines that endogenously overexpress Muc1 (Fig. 4c). Control experiments with NK-92 cells equipped with catalytically dead StcE E447D mucinase confirmed that the enzymatic activity of StcE was required for the enhancement in cytotoxicity (Fig. 4d). Additional controls indicated that the tethering of StcE to the NK-92 cell surface was required for the enhanced cytotoxicity against mucin-expressing targets. The cytolytic activity of NK-92 cells was not significantly enhanced by treatment with StcE ΔX409, which was catalytically active but did not remain tethered to the NK-92 cell surface after rinsing (Fig. 4d and Extended Data Fig. 8a). The inability of StcE ΔX409 treatment to enhance the cytolytic activity of NK-92 cells indicated that the StcE mucinase treatment probably did not directly enhance the latent activity of NK-92 cells through the trimming of their mucin-domain proteins (Fig. 4d).

We observed a localized disruption of the mucin barrier at the interface between StcE-equipped NK-92 cells and target cells. Visible deflection of microvilli on 1E7 cells in the contact zone with both unmodified NK-92 and StcE NK-92 indicated that both wild-type and engineered cells could form viable mechanical connections with the target cells (Fig. 4e). However, a high density of Muc1-GFP and microvilli persisted in the contact zone with unmodified NK-92 cells (Fig. 4e). Lower Muc1-GFP levels and fewer microvilli were observed in the contact zone with StcE NK-92 cells (Fig. 4e,f). These results were consistent with the surface-tethered StcE locally cleaving the mucin or otherwise aiding in the segregation of cell-surface mucin from the contact interface, as well as disrupting the microvilli.

We next compared the killing efficiency of the StcE NK-92 cells with HER2 CAR NK-92 cells and StcE CAR NK-92 cells, which were equipped with both HER2 CAR and StcE mucinase. The engineered NK-92 cells were tested against 1E7 *HER2* OE cells, as well as the SKOV3 ovarian and SKBR3 breast cancer cell lines, which endogenously express HER2 and cell-surface mucins, including Muc1 (refs. 43–45). The thickness of the glycocalyx was reduced in 1E7 cells and two cancer cell lines following treatment with recombinant StcE (Fig. 4g). Equipping the NK-92 cells with StcE, HER2 CAR or both enhanced their cytotoxicity against the 1E7 and cancer cell lines (Fig. 4h). The most significant enhancement was observed for NK-92 cells equipped with both StcE and HER2 CAR (Fig. 4h). The SKOV3 cells had a thick glycocalyx of approximately 120 nm that was reduced to approximately 60 nm following mucinase treatment, consistent with the pronounced benefit of StcE equipment for killing the SKOV3 targets. (Fig. 4g,h).

Modular strategy for displaying GE enzymes

To improve the coupling of StcE to the NK cell surface, we developed a modular strategy for the surface display of StcE or other GE enzymes. Inspired by a modular design for universal CARs[46], we developed a strategy to anchor GE enzymes to the NK-92 surface through leucine-zipper-mediated coupling. The RR leucine zipper was genetically expressed on the NK-92 cell surface as a fusion protein with an ALFA-tag, a transmembrane anchor and an sfGFP fluorescent marker to create Zip-NK-92 cells (Fig. 5a,b). The X409 lectin domain of StcE was swapped for the EE leucine zipper and the new fusion protein, StcE-EE, was recombinantly produced (Fig. 5a). We confirmed that StcE-EE could cleave Muc1 from the cell surface similar to wild-type StcE (Extended Data Fig. 8a). StcE-EE coupled to the Zip-NK-92 cell surface with nanomolar affinity (effective $K_d \approx 3.26$ nM) and did not significantly affect the Zip-NK-92 cell viability (Fig. 5c and Extended Data Fig. 8b). Coupling with StcE-EE enhanced the cell-mediated cytotoxicity against Muc1-expressing B2 cells and five Muc1-expressing cancer cell lines that we tested: breast SKBR3, pancreatic Capan-2, breast KPL-1, breast T47D and breast ZR-75-1 (Fig. 5d–f).

To validate the modularity of the enzyme-tethering strategy and further test the concept of GE NK cells, we generated a recombinant sialidase that was fused to the EE leucine zipper for coupling to Zip-NK-92 cells. We chose the pan-specific *Salmonella typhimurium* sialidase, which trims sialic acids with α2,3, α2,6 and α2,8 linkages. The coupling of sialidase-EE to Zip-NK-92 mediated a small increase in cytotoxicity against Muc1-expressing B2 compared with control Zip-NK-92 cells (Extended Data Fig. 8c). However, the surface-displayed sialidase markedly increased the NK-92-cell-mediated cytotoxicity against the cancer cell lines that we tested (Fig. 5f). Overall, our results indicate that the surface display of GE enzymes on effector cells could be an alternative or complementary strategy to CARs for enhancing the cell-mediated cytotoxicity against cancer cells.

Outlook

Equipping effector immune cells with surface-displayed or secreted enzymes that disrupt the glycocalyx structure represents an attractive strategy for the enhanced killing of tumour cells, especially if selective mucinases that preferentially cleave cancer-associated mucins can be identified or developed through protein engineering[47]. Pharmacological agents or metabolic inhibitors that disrupt the synthesis of a protective glycocalyx in cancer cells also have the potential to improve current immunotherapies when co-administered. From the perspective of personalized medicine, mucin transcript levels, allele lengths and surface levels are experimentally measurable quantities in patient samples. Combined with the physical understanding developed here, such metrics might inform the likelihood of recalcitrance to immune cell therapies. The underlying mechanisms of protection by the mucin layer may be multifaceted. Possible actions include changes in target-cell-surface topography and ligand presentation by mucins, as well as the regulation of biomolecular processes that may be sensitive to macromolecular crowding and spatial constraints imposed by mucins at the immune cell surface[5,10,48]. Unravelling these mechanisms has the potential to accelerate the discovery of therapeutic interventions that overcome the mucin barrier of cancer cells.

Online content

Any methods, additional references, Nature Portfolio reporting summaries, source data, extended data, supplementary information, acknowledgements, peer review information; details of author contributions and competing interests; and statements of data and code availability are available at https://doi.org/10.1038/s41563-024-01808-0.

References

1. Shimasaki, N., Jain, A. & Campana, D. NK cells for cancer immunotherapy. *Nat. Rev. Drug Discov.* **19**, 200–218 (2020).
2. Heczey, A. et al. Anti-GD2 CAR-NKT cells in relapsed or refractory neuroblastoma: updated phase 1 trial interim results. *Nat. Med.* **29**, 1379–1388 (2023).
3. June, C. H., O'Connor, R. S., Kawalekar, O. U., Ghassemi, S. & Milone, M. C. CAR T cell immunotherapy for human cancer. *Science* **359**, 1361–1365 (2018).
4. Ghasempour, S. & Freeman, S. A. The glycocalyx and immune evasion in cancer. *FEBS J.* **290**, 55–65 (2021).
5. Möckl, L. The emerging role of the mammalian glycocalyx in functional membrane organization and immune system regulation. *Front. Cell Dev. Biol.* **8**, 253 (2020).
6. Zhou, J. Y. & Cobb, B. A. Glycans in immunologic health and disease. *Annu. Rev. Immunol.* **39**, 511–536 (2021).
7. Fernandes, Â. et al. Glycans as shapers of tumour microenvironment: a sweet driver of T-cell-mediated anti-tumour immune response. *Immunology* **168**, 217–232 (2023).
8. van de Wiel-van Kemenade, E. et al. Episialin (MUC1) inhibits cytotoxic lymphocyte-target cell interaction. *J. Immunol.* **151**, 767–776 (1993).
9. Hollingsworth, M. A. & Swanson, B. J. Mucins in cancer: protection and control of the cell surface. *Nat. Rev. Cancer* **4**, 45–60 (2004).
10. Shurer, C. R. et al. Physical principles of membrane shape regulation by the glycocalyx. *Cell* **177**, 1757–1770.e21 (2019).
11. Paszek, M. J. et al. The cancer glycocalyx mechanically primes integrin-mediated growth and survival. *Nature* **511**, 319–325 (2014).
12. Kuo, J. C.-H., Gandhi, J. G., Zia, R. N. & Paszek, M. J. Physical biology of the cancer cell glycocalyx. *Nat. Phys.* **14**, 658–669 (2018).
13. Bell, G. I., Dembo, M. & Bongrand, P. Cell adhesion. Competition between nonspecific repulsion and specific bonding. *Biophys. J.* **45**, 1051–1064 (1984).
14. Suzuki, Y., Sutoh, M., Hatakeyama, S. & Mori, K. MUC1 carrying core 2 O-glycans functions as a molecular shield against NK cell attack, promoting bladder tumor metastasis. *Int. J. Oncol.* **40**, 1831–1838 (2012).
15. Okamoto, T. et al. Core2 O-glycan-expressing prostate cancer cells are resistant to NK cell immunity. *Mol. Med. Rep.* **7**, 359–364 (2013).
16. Madsen, C. B. et al. Glycan elongation beyond the mucin associated Tn antigen protects tumor cells from immune-mediated killing. *PLoS ONE* **8**, e72413 (2013).
17. Tsuboi, S. et al. A novel strategy for evasion of NK cell immunity by tumours expressing core2 O-glycans. *EMBO J.* **30**, 3173–3185 (2011).
18. Ajo-Franklin, C. M., Ganesan, P. V. & Boxer, S. G. Variable incidence angle fluorescence interference contrast microscopy for *z*-imaging single objects. *Biophys. J.* **89**, 2759–2769 (2005).

19. Lambacher, A. & Fromherz, P. Fluorescence interference-contrast microscopy on oxidized silicon using a monomolecular dye layer. *Appl. Phys. A* **63**, 207–216 (1996).
20. Paszek, M. J. et al. Scanning angle interference microscopy reveals cell dynamics at the nanoscale. *Nat. Methods* **9**, 825–827 (2012).
21. Colville, M. J., Park, S., Zipfel, W. R. & Paszek, M. J. High-speed device synchronization in optical microscopy with an open-source hardware control platform. *Sci. Rep.* **9**, 12188 (2019).
22. Colville, M., Park, S., Singh, A., Paszek, M. & Zipfel, W. R. Azimuthal beam scanning microscope design and implementation for axial localization with scanning angle interference microscopy. in *Biomedical Engineering Technologies. Methods in Molecular Biology* Vol. 2393, 127–152 (Springer, 2022).
23. Nason, R. et al. Display of the human mucinome with defined O-glycans by gene engineered cells. *Nat. Commun.* **12**, 4070 (2021).
24. Lan, Y., Ni, W. & Tai, G. Expression of MUC1 in different tumours and its clinical significance (review). *Mol. Clin. Oncol.* **17**, 161 (2022).
25. Carson, D. D. The cytoplasmic tail of MUC1: a very busy place. *Sci. Signal.* **1**, pe35 (2008).
26. Tang, X. et al. First-in-man clinical trial of CAR NK-92 cells: safety test of CD33-CAR NK-92 cells in patients with relapsed and refractory acute myeloid leukemia. *Am. J. Cancer Res.* **8**, 1083–1089 (2018).
27. Arai, S. et al. Infusion of the allogeneic cell line NK-92 in patients with advanced renal cell cancer or melanoma: a phase I trial. *Cytotherapy* **10**, 625–632 (2008).
28. Williams, B. A. et al. A phase I trial of NK-92 cells for refractory hematological malignancies relapsing after autologous hematopoietic cell transplantation shows safety and evidence of efficacy. *Oncotarget* **8**, 89256–89268 (2017).
29. Yu, A. C. Y., Worrall, L. J. & Strynadka, N. C. J. Structural insight into the bacterial mucinase StcE essential to adhesion and immune evasion during enterohemorrhagic *E. coli* infection. *Structure* **20**, 707–717 (2012).
30. Walsh, M. D., Luckie, S. M., Cummings, M. C., Antalis, T. M. & McGuckin, M. A. Heterogeneity of MUC1 expression by human breast carcinoma cell lines in vivo and in vitro. *Breast Cancer Res. Treat.* **58**, 255–266 (1999).
31. van de Wall, S., Santegoets, K. C. M., van Houtum, E. J. H., Büll, C. & Adema, G. J. Sialoglycans and siglecs can shape the tumor immune microenvironment. *Trends Immunol.* **41**, 274–285 (2020).
32. Hudak, J. E., Canham, S. M. & Bertozzi, C. R. Glycocalyx engineering reveals a Siglec-based mechanism for NK cell immunoevasion. *Nat. Chem. Biol.* **10**, 69–75 (2014).
33. Rosenstock, P., Horstkorte, R., Gnanapragassam, V. S., Harth, J. & Kielstein, H. Siglec-7 expression is reduced on a natural killer (NK) cell subset of obese humans. *Immunol. Res* **65**, 1017–1024 (2017).
34. Gandhi, J. G., Koch, D. L. & Paszek, M. J. Equilibrium modeling of the mechanics and structure of the cancer glycocalyx. *Biophys. J.* **116**, 694–708 (2019).
35. de Gennes, P. G. Polymers at an interface; a simplified view. *Adv. Colloid Interface Sci.* **27**, 189–209 (1987).
36. Paturej, J., Sheiko, S. S., Panyukov, S. & Rubinstein, M. Molecular structure of bottlebrush polymers in melts. *Sci. Adv.* **2**, e1601478 (2016).
37. Kudelka, M. R. et al. Cellular O-glycome reporter/amplification to explore O-glycans of living cells. *Nat. Methods* **13**, 81–86 (2016).
38. Argüeso, P. et al. Association of cell surface mucins with galectin-3 contributes to the ocular surface epithelial barrier. *J. Biol. Chem.* **284**, 23037–23045 (2009).
39. Lang, M., Hoffmann, M., Dockhorn, R., Werner, M. & Sommer, J.-U. Fluctuation driven height reduction of crosslinked polymer brushes: a Monte Carlo study. *J. Chem. Phys.* **139**, 164903 (2013).
40. Olguin-Olguin, A. et al. Chemokine-biased robust self-organizing polarization of migrating cells in vivo. *Proc. Natl Acad. Sci. USA* **118**, e2018480118 (2021).
41. Zhang, C. et al. Chimeric antigen an off-the-shelf cellular therapeutic for targeted elimination of cancer cells and induction of protective antitumor immunity. *Front. Immunol.* **8**, 533 (2017).
42. Malaker, S. A. et al. The mucin-selective protease StcE enables molecular and functional analysis of human cancer-associated mucins. *Proc. Natl Acad. Sci. USA* **116**, 7278–7287 (2019).
43. Wang, L. et al. Monoclonal antibody targeting MUC1 and increasing sensitivity to docetaxel as a novel strategy in treating human epithelial ovarian cancer. *Cancer Lett.* **300**, 122–133 (2011).
44. Cipollone, J. A. et al. The anti-adhesive mucin podocalyxin may help initiate the transperitoneal metastasis of high grade serous ovarian carcinoma. *Clin. Exp. Metastasis* **29**, 239–252 (2012).
45. Singh, R. et al. Target-specific cytotoxic activity of recombinant immunotoxin scFv(MUC1)-ETA on breast carcinoma cells and primary breast tumors. *Mol. Cancer Ther.* **6**, 562–569 (2007).
46. Cho, J. H., Collins, J. J. & Wong, W. W. Universal chimeric antigen receptors for multiplexed and logical control of T cell responses. *Cell* **173**, 1426–1438.e11 (2018).
47. Pedram, K. et al. Design of a mucin-selective protease for targeted degradation of cancer-associated mucins. *Nat. Biotechnol.* https://doi.org/10.1038/s41587-023-01840-6 (2023).
48. Zhou, H.-X., Rivas, G. & Minton, A. P. Macromolecular crowding and confinement: biochemical, biophysical, and potential physiological consequences. *Annu. Rev. Biophys.* **37**, 375–397 (2008).

Methods

Primary cells and cell lines

MCF10A cells were cultured in Dulbecco's modified Eagle's medium (DMEM)/F12 media (Thermo Fisher Scientific) supplemented with 5% horse serum (Thermo Fisher Scientific), 20 ng ml^{-1} epidermal growth factor (PeproTech), 10 mg ml^{-1} insulin (Sigma), 500 ng ml^{-1} hydrocortisone (Sigma), 100 ng ml^{-1} cholera toxin (Sigma) and 1× penicillin/streptomycin (Thermo Fisher Scientific) at 37 °C in 5% CO_2. HEK293T cells (gift from V. Weaver) were cultured in DMEM high-glucose media (Thermo Fisher Scientific) supplemented with 10% foetal bovine serum (Thermo Fisher Scientific) and 1× penicillin/streptomycin at 37 °C in 5% CO_2. ZR-75-1 (ATCC; CRL-1500), T47D (ATCC; HTB-133), SKBR3 (gifted by J. Lammerding), KPL-1 (DSMZ; ACC 317) and Capan-2 (ATCC; HTB-80) cells were cultured in RPMI 1640 media (Thermo Fisher Scientific) supplemented with 10% foetal bovine serum and 1× penicillin/streptomycin at 37 °C in 5% CO_2. SKOV3 (ATCC; HTB-77) was cultured in McCoy's 5A (Modified) Medium (Thermo Fisher Scientific) supplemented with 10% foetal bovine serum and 1× penicillin/streptomycin at 37 °C in 5% CO_2. NK-92 cells (ATCC; CRL-2407) were cultured in α-MEM without ribonucleosides media (Thermo Fisher Scientific) supplemented with 12.5% foetal bovine serum, 12.5% horse serum, 0.20 mM Myo-inositol (Sigma-Aldrich), 0.10 mM 2-mercaptoethanol (Thermo Fisher Scientific), 0.02 mM folic acid (Millipore Sigma), 100 U ml^{-1} recombinant human IL-2 (PeproTech) and 1× penicillin/streptomycin at 37 °C in 5% CO_2. Human CD19 CAR T cells and HER2 CAR T cells were cultured in RPMI 1640 media supplemented with 10% foetal bovine serum, 20 mM HEPES buffer (Gibco), 1% MEM Non-Essential Amino Acids (Gibco), 50 μM 2-mercaptoethanol, 80 U ml^{-1} recombinant human IL-2 and 1× penicillin at 37 °C in 5% CO_2. Equine PBMCs were cultured in DMEM high-glucose media supplemented with 10% foetal bovine serum and 1× penicillin/streptomycin at 37 °C in 5% CO_2. Primary human NK cells were cultured in RPMI 1640 media supplemented with 10% foetal bovine serum, 1× penicillin/streptomycin and 100 U ml^{-1} IL-2 at 37 °C in 5% CO_2.

Cloning and constructs

Supplementary Tables 2 and 3 lists the sequences for cDNAs, primers and homology-directed repair (HDR) templates in this work. The cDNAs for Muc1 and Muc1-mOxGFP (referred to as Muc1-GFP here), as well as the Muc1 constructs with varying numbers of TR, were previously cloned into a PiggyBac expression system containing a tetracycline-inducible promoter ($P_{CMV\text{-}min}$-$tetO_7$) and a separate puromycin selection cassette (pPB tetOn PuroR)[10,49]; all of the mucin constructs had the native Muc1 cytoplasmic tail deleted. Lentiviral plasmids for the constitutive expression of human *GCNT1*, *LGALS3*, *HER2* and *CD19*, as well as genes for cytoplasmic mScarlet-I, were prepared by inserting the cDNAs in place of GFP in pLenti CMV GFP Hygro (Addgene no. 17446), using the BamHI & BsrGI or BamHI & SalI restriction sites. The *GCNT1* and *CD19* cDNAs were generated by custom gene synthesis (General Biosystems and Twist Bioscience, respectively). The cDNA for mScarlet-I with a nuclear export signal (LQKKLEELELD) was synthesized as a gBlock gene fragment (Integrated DNA Technologies). The human *HER2* cDNA was amplified by PCR from the plasmid, *HER2* WT (Addgene no. 16257), with primers that added 5′ BamHI and 3′ BsrGI restriction sites. The cDNA for human *LGALS3* was similarly amplified by PCR from a pET21a expression vector (gift from C. Bertozzi). The lentiviral vector for the second-generation HER2-specific CAR[50] that was expressed in NK-92 cells was synthesized by custom gene synthesis (Twist Bioscience) and inserted in place of GFP in pLenti CMV GFP Hygro. The pHR lentiviral vectors for the expression of the third-generation CD19-specific CAR[51] in NK-92 cells were gifted by X. Su. Lentiviral vectors for the second-generation HER2 and CD19 CARs that were expressed in primary T cells were gifted by M. Kim. A pLentiCRISPR V2 hygro plasmid (Addgene no. 98291) for the KO of *GNE* was created by annealing the oligos 5′-CACCGACATCAAGTTCAAAGAACTC-3′ and 5′-AAACGAGTTCTTTGAACTTGATGTC-3′, and inserting into the BsmBI restriction site. Recombinant GFP nanobody cDNA (PDB no. 3OGO_E) was generated by custom gene synthesis (Integrated DNA Technologies) and cloned into the BamHI and HindIII restriction sites of pTP1112 (Addgene no. 104158). The cDNA for the cell-surface display of a leucine zipper (RR)—including an IgK leader, ALFA-tag, leucine zipper, Myc tag, PDGFRβ transmembrane domain and cytoplasmic sfGFP—was synthesized by custom gene synthesis and inserted by the manufacturer into pTwist SFFV Puro (Twist Bioscience).

Generation of mucin-expressing and glycoengineered MCF10A cell lines

MCF10A cells stably expressing the rtTA-M2 tetracycline transactivator were prepared by lentiviral transduction using the pLV rtTA-NeoR plasmid, as previously described[20]. For the preparation of mucin-expressing cell lines, MCF10A rtTA-M2 cells were co-transfected with the PiggyBac hyperactive transposase and PiggyBac plasmids containing ITR-flanked expression cassettes (that is, pPB tetOn PuroR plasmids) using the NEPA21 Electroporator (NEPAGENE) and subsequently selected with 1 μg ml^{-1} puromycin. The stable MCF10A lines expressing Muc1 and Muc1-GFP were clonally expanded by limiting the dilution of single cells in 96-well plates. Individual clones were isolated that exhibited low leaky expression and titratable surface levels of Muc1 (for example, B2 clonal lines) and Muc1-GFP (for example, 1E7 clonal line).

Cell lines overexpressing *GCNT1*, *LGALS3*, *HER2*, *CD19* and the gene for mScarlet-I were prepared by transduction with lentiviral particles generated in HEK293T using the pLenti CMV Hygro plasmids HEK293T cells following previously described methods[20]. Cell selection was with 200 μg ml^{-1} hygromycin, and mScarlet-I cells were additionally sorted by fluorescence-activated cell sorting. The KO of *GNE* in the 1E7 clone was achieved by lentiviral transduction using the pLentiCRISPR V2 system and selection with 200 μg ml^{-1} hygromycin, as previously described[10]. The selected cells were clonally expanded by limiting dilution in 96-well plates, and individual clones were screened for the homozygous KO of *GNE* by Sanger sequencing of genomic DNA that was isolated using the Quick-DNA MiniPrep Kit (Zymo, D3024). The KO of *C1GALT1* in 1E7 cells was achieved using the Alt-R CRISPR/Cas9 system (Integrated DNA Technologies) with HDR templates that introduced an in-frame stop codon and an EcoRI restriction site for screening (Supplementary Table 3). CRISPR/Cas9 editing was conducted according to the manufacturer's protocol for the Alt-R system. Briefly, 1E7 cells were transfected with precomplexed crRNA and ATTO550-tracrRNA, along with the HDR template, using electroporation. After 48 h, transfected 1E7 cells were clonally expanded by limiting dilution in 96-well plates. To screen for successful KOs, genomic regions encompassing the targeted CRISPR/Cas9 cut sites were amplified by PCR and analysed by EcoRI restriction digest and Sanger sequencing.

Generation of engineered and reporter NK-92 cell lines

HER2 CAR NK-92 and CD19 CAR NK-92 cells were generated from NK-92 cells through the lentiviral transduction of transgenes for the second-generation HER2 CAR[50] (FRP5 scFv, CD8α hinge, CD28 transmembrane domain, CD28 co-stimulatory domain and CD3ζ signalling domain, followed by a P2A sequence and mTagBFP2) or third-generation CD19 CAR[51] (FMC63 scFv, stalk and transmembrane domain from CD8α, CD28 and 4-1BB co-stimulatory domains, and CD3ζ signalling domain, followed by an in-frame sfGFP tag). Zip-NK-92 cells were generated by the lentiviral transduction of NK-92 cells with the transgene for the surface-displayed leucine zipper (RR) with the sfGFP tag. Lentivirus was prepared in HEK293T cells following standard protocols[52]. All the CARs and Zip-NK-92 cells were sorted for high BFP or GFP signals.

A NK-92 Gzmb-Gamillus knock-in cell line was generated using the IDT Alt-R CRISPR/Cas9 system to insert a GGSGGSGGS linker and the highly acid-tolerant green fluorescent protein (Gamillus) directly before the stop codon in the endogenous *GZMB* locus[53,54].

A double-stranded DNA HDR template encoding the linker and fluorescent protein flanked by 200 bp homology arms was ordered from Integrated DNA Technologies as an Alt-R HDR Donor Block. CRIPSR-Cas9 editing was conducted according to the manufacturer's instructions. Cells that successfully incorporated Gamillus were enriched by two rounds of fluorescence-activated cell sorting.

Preparation of StcE NK-92 and enzyme-coupled Zip-NK-92 cells

To prepare StcE NK-92 cells, wild-type NK-92 cells were incubated at 0.1–0.4 × 10^6 cells ml^{-1} with 100 nM recombinant StcE in an NK-92 cell culture medium at 37 °C for 1 h. Cells were subsequently washed twice by centrifugation at 400*g* for 5 min and the cell pellets were resuspended in the NK-92 cell culture medium to remove unbound StcE. HER2 CAR NK cells with surface-tethered StcE (StcE HER2 CAR NK-92) were similarly prepared. The cells were analysed or used in cytotoxicity assays immediately following preparation. For the preparation of GE NK cells, Zip-NK-92 cells were incubated at 0.1–0.4 × 10^6 cells ml^{-1} with 10 nM recombinant StcE or sialidase leucine zipper fusion proteins (StcE-EE and sialidase-EE, respectively) in the NK-92 cell culture medium at 37 °C for 1 h. The cells were gently agitated several times during incubation. The cells were then washed twice by centrifugation at 400*g* for 5 min and the cell pellets were resuspended in the NK-92 cell culture medium to remove unbound enzymes and immediately used. Bound enzyme levels on the Zip-NK-92 cells were confirmed by flow cytometry using the anti-His-tag antibody.

Preparation of CAR T cells

CAR T cells were prepared through lentiviral transduction with transgenes for the second-generation HER2 CAR (Herceptin scFv, CD8α hinge, CD28 transmembrane domain, CD28 co-stimulatory domain and CD3ζ signalling domain) or CD19 CAR (FMC63 scFv, CD8α hinge, CD8α transmembrane domain, 4-1BB co-stimulatory domain and CD3ζ signalling domain). Human T cells were isolated from healthy donor peripheral blood using the EasySep CD8 T-cell isolation kit (STEMCELL). Human T cells were activated for 24 h using human CD3/CD28 Dynabeads per the manufacturer's protocol (Thermo Fisher Scientific) and cultured in a complete RPMI medium supplemented with 80 U ml^{-1} IL-2. The retrovirus was generated using the Lenti-X packaging cell line (Takara). Lenti-X cells were plated at 0.9 × 10^6 cells per well in a six-well plate. The following day, the Lenti-X cells were transfected with CAR lentiviral plasmids plus LV-MAX lentiviral packaging mix (Thermo Fisher Scientific) using Lipofectamine 2000 according to the manufacturer's protocol. The media were swapped 6 h post-transfection. Filtered (0.45 µm) retroviral-containing supernatants were collected 24 and 48 h post-transfection. For T-cell transduction, 1 × 10^6 activated CD8 T cells were plated on RetroNectin (Takara)-coated 12-well plates (10 µg ml^{-1}) with retrovirus-containing supernatants, supplemented with 80 U ml^{-1} IL-2, and spun twice at 37 °C both 24 and 48 h post-transfection at 2,500 r.p.m. T cells were then detached from RetroNectin at least 24 h post-transduction and analysed for CAR expression using Myc tag by flow cytometry.

Isolation of primary human NK cells and PBMCs

Buffy coats of healthy donors were procured as de-identified products from the New York Blood Center. Human PBMCs were isolated from buffy coats by density-gradient centrifugation using Ficoll-Paque PLUS (GE Healthcare). Primary NK cells were extracted from PBMCs by negative immunomagnetic isolation using an NK cell isolation kit (no. 130-092-657; Miltenyi Biotec) according to the manufacturer's protocol. Recovered human NK cells were cultured in RPMI 1640 media supplemented with 10% foetal bovine serum, 1× penicillin/streptomycin and 100 U ml^{-1} IL-2 at 37 °C in 5% CO_2. The purity of the NK cell population was validated by flow cytometry using PE-Vio 770-CD56 and FITC-CD3.

Isolation of equine PBMCs

Equine PBMCs were isolated from three adult light-breed horses with institutional approval (Cornell Institutional Animal Care and Use Committee no. 2018-0024). Blood (50 ml) was collected from the jugular vein using a 20-gauge needle into heparinized blood tubes (BD) and stored on ice. PBMCs and plasma were allowed to separate from the granulocytes and red blood cells. Density-gradient centrifugation was performed using Ficoll-Paque PLUS (GE Healthcare) at 900*g* for 20 min at 10 °C. The PBMCs were collected from the plasma–Ficoll interface with a sterile Pasteur pipette and resuspended in 20 ml phosphate-buffered saline (PBS). An additional centrifugation at 500*g* for 15 min was performed to wash the cells, and then the resulting cell pellet was resuspended in an additional 20 ml PBS and centrifuged at 100*g* for 10 min to remove additional platelets. The final cell pellet was resuspended in growth media for cell counting and culture.

Western blot analysis

Cells were plated and induced with 1 µg ml^{-1} doxycycline (204734, Santa Cruz Biotechnology) for 24 h before lysis with RIPA buffer (89900, Thermo Fisher Scientific) with Halt Protease and Phosphatase Inhibitor Cocktail (78446, Thermo Fisher Scientific). The lysates were separated on NuPAGE 3–8% Tris-Acetate gels or NuPAGE 4–12% Bis-Tris gels and transferred to low-fluorescence polyvinylidene fluoride membranes (Millipore Sigma, IPFL07810). Primary antibodies were diluted at 1:500 in 5% BSA TBST and fluorophore-conjugated or biotinylated lectins were diluted to 2 µg ml^{-1} in 5% BSA TBST and incubated overnight at 4 °C. Secondary antibodies and Neutravidin-DyLight 800 were diluted at 1:1,000 or 1 µg ml^{-1} in 5% BSA TBST and incubated for 1 h at room temperature. The blots were imaged on a ChemiDoc MP Imaging System (Bio-Rad).

Labelling and analysis of cell-surface epitopes and glycans

For the Muc1 and lectin staining of 1E7 and glycoengineered progeny, the cells were plated on culture dishes, grown for 24 h and then induced with various concentrations of doxycycline for 24 h. CF640R PNA and biotin MAL-II were diluted at 1:200 in 0.5% BSA PBS and incubated with trypsinized cells at 4 °C for 1 h for each stain. Secondary labelling was performed with neutravidin-conjugated DyLight 650, diluted at 1:200 in 0.5% BSA PBS and incubated with cells at 4 °C for 1 h. For the analysis of cell-surface expression level of Muc1-GFP, the GFP-nanobody-conjugated Alexa Fluor 647 was diluted at 1:200 in 0.5% BSA PBS and incubated with cells at 4 °C for 1 h. For the analysis of cell-surface expression level of Muc1, anti-human Muc1 clone HMPV (555925, BD Biosciences) was diluted at 1:200 in 0.5% BSA PBS and incubated with cells at 4 °C for 1 h. Secondary labelling was performed with Alexa Fluor 647-conjugated goat anti-mouse, diluted at 1:200 in 0.5% BSA PBS and incubated with cells at 4 °C for 1 h.

For detecting StcE and StcE-Zip levels on the NK-92 surface, anti-His-tag antibody was diluted at 1:100 in 0.5% BSA PBS and incubated with suspended cells at 4 °C for 1 h. Secondary labelling was performed with Alexa Fluor 647 goat anti-rabbit IgG, diluted at 1:500 in 0.5% BSA PBS and incubated with cells at 4 °C for 1 h.

For detecting Siglec-7 and Siglec-9 on NK cells, PE-Vio 770 anti-human CD56 (1:50), FITC anti-human CD3 (1:50), APC anti-human CD328 (1:100) and anti-human Siglec-9 (1:100) was diluted in 0.5% BSA PBS and incubated with primary NK cells and NK-92 cell lines at 4 °C for 1 h. As a secondary label for anti-human Siglec-9, Alexa Fluor 647-conjugated goat anti-mouse was diluted at 1:200 in 0.5% BSA PBS and incubated with cells at 4 °C for 1 h.

For all the samples, flow cytometry was performed on an Attune NxT flow cytometry instrument (Thermo Fisher Scientific). Supplementary Figs. 1–3 present the gating strategies for all the flow cytometry analyses in this work.

Immunofluorescence

The 1E7 cells and sublines were plated in 35 mm glass-bottom dishes (P35G-1.5-14-C; Mattek), grown for 24 h and then induced with various concentrations of doxycycline for 24 h. The cells were fixed with 4.0% paraformaldehyde and permeabilized with 0.1% Triton X-100. Anti-GCNT1 antibody was diluted at 1:50 in 0.5% BSA PBS and incubated on samples at 4 °C for 1 h. Secondary labelling was performed with an anti-rabbit Alexa Fluor 647 conjugate diluted at 1:200 in 0.5% BSA PBS and incubated with cells at 4 °C for 1 h. Anti-Gal-3 antibody (sc-19280, Santa Cruz Biotechnology) was diluted at 1:50 in 0.5% BSA PBS and incubated with the 1E7 clone at 4 °C for 1 h. Secondary labelling was performed with a rabbit anti-goat IgG Alexa Fluor 647 conjugate diluted at 1:200 in 0.5% BSA PBS and incubated with cells at 4 °C for 1 h. In some experiments, where indicated, TD139 (28400, Cayman Chemical) was diluted to 1, 10 and 50 µM in MCF10A cell culture media with 1,000 ng ml^{-1} of doxycycline and incubated with 1E7 cells at 37 °C for 2 h before fixation, permeabilization and galectin staining. Muc1 was labelled in unfixed B2 clonal cells with anti-Muc1 Janelia Fluor 549 (NBP-2-47883JF549; Novus Biologicals) diluted at 1:200 in 0.5% BSA PBS and incubated with the cells at 4 °C for 1 h. All the samples above were imaged on an LSM 800 confocal microscope using ×10 (numerical aperture, 0.3; air), ×20 (numerical aperture, 0.8; air) or ×63 (numerical aperture, 1.2; water) objectives (ZEISS).

Analysis of galectin binding

The 1E7 cells and sublines were plated in 35 mm glass-bottom dishes (P35G-1.5-14-C; Mattek), grown for 24 h and then induced with 1,000 ng ml^{-1} of doxycycline for 24 h. The cells were treated with a control buffer or 5,000 U ml^{-1} PNGase F for 1 h before galectin binding analysis. Alexa Flour 568-conjugated recombinant human Gal-1 and Gal-3 were diluted in 0.5% BSA PBS and incubated with 1E7 and sublines at 4 °C for 1 h. Cells were washed three times with 0.5% BSA PBS to remove any unbound galectins and then imaged on an LSM 800 confocal microscope using a ×63 (numerical aperture, 1.2; water) objective (ZEISS). Cell-surface fluorescence was quantified using ImageJ software (v1.53s) by averaging the intensity values from a 20 × 20 pixel^2 subregion in each cell.

Live-cell imaging

The 1E7 cells were plated in 35 mm glass-bottom dishes, grown for 24 h and then induced with various concentrations of doxycycline for 24 h. Co-cultures of the 1E7 cells with NK-92, StcE NK-92 or NK-92 GzmB-Gamillus cells were prepared by adding the immune cells to the plated 1E7 cells and incubating for 4 h before imaging. For these experiments, StcE NK cells were prepared as described above, with the exception that NK-92 cells were incubated with 100 nM StcE for 1 h at 37 °C before washing with phenol-red-free MCF10A cell culture media. For the assessment of soluble StcE activity and specificity, the 1E7 cells in glass-bottom dishes were treated with 100 nM recombinant StcE, mutant StcE or StcE-EE in MCF10A culture media for 1 h at 37 °C and labelled with Alexa Fluor 647-conjugated GFP nanobody before imaging. All the samples above were imaged at 37 °C and under 5% CO_2 conditions. For labelling cytolytic granules in live NK-92 GzmB-Gamillus cells, the immune cells were incubated with 100 nM LysoTracker Deep Red (L12492; Thermo Fisher Scientific) in NK-92 cell culture media for 30 min at 37 °C. After washing with cold PBS, the cells were plated in 35 mm glass-bottom dishes with 0.5% BSA PBS before imaging. All of the imaging was conducted on an LSM 800 confocal microscope using a ×63 (numerical aperture, 1.2; water) objective (ZEISS).

Cytotoxicity assays

Target MCF10A cells and derivative cell lines (for example, 1E7 and B2 clonal cells) were fluorescently labelled by incubation with 10 µM CellTracker Green CMFDA Dye (Invitrogen) in MCF10A growth media for 15 min. Cancer cell lines were similarly labelled with 10 µM CellTracker Green CMFDA in each cell line's respective culture media. Also, 4 × 10^4 labelled target cells were suspended with varying ratios of effector (NK or T) cells in 200 µl of growth media of the target cell line in the absence of IL-2 and co-cultured in an ultralow-attachment U-bottom 96-well plate (Corning) for 4 h at 37 °C in 5% CO_2. After 4 h, propidium iodide (PI; 20 µg ml^{-1}, Sigma) was added to each well for 10 min. Cell-mediated cytotoxicity was evaluated by flow cytometry, as previously described[32,55]. At least 1 × 10^4 target cells were analysed after electronic gating on CellTracker Green. Percentage cytotoxicity was calculated as 100 × (experimental % dead − spontaneous % dead)/(100 − spontaneous % dead), where experimental % dead is the percentage of PI-positive target cells in co-cultures and spontaneous % dead is the percentage of PI-positive control target cells cultured in the absence of effector cells.

In some experiments, where indicated, the cells were sorted by Muc1 expression or treated with 100 nM StcE for 1 h at 37 °C before the cytotoxicity assays. For sorting, ZR-75-1 cells were labelled with anti-human Muc1 Janelia Fluor 549 (NBP-2-47883JF549, Novus Biologicals) diluted at 1:200 in 0.5% BSA PBS at 4 °C for 1 h and sorted the cells with defined standardized gates for low, intermediate and high Muc1 expression by fluorescence-activated cell sorting (Sony MA900 Cell Sorter). In place of PI, ZR-75-1 cells were labelled with annexin V conjugated with CF647 (0.5 µg ml^{-1}, Biotium) and diluted in HEPES-buffered saline containing 2.5 mM calcium chloride, which was added to each well for 15 min. Cytotoxicity based on annexin V staining was assessed as described above for PI.

Granule polarization analysis

The calculation of protein polarization was performed by using MATLAB (R2019a), as previously reported[40]. Briefly, a mask for the target cells was created by outlining the cell on the bright-field image. The centre of cells was determined by averaging the positions of all the pixels inside the cell. The centre of Gamillus was determined by a weighted average over all the pixel positions using the Gamillus intensity as weight and normalizing by the sum of all the Gamillus intensities. A polarity vector was defined as the arrow from the centre position of cells to the centre position of Gamillus. A scalar polarization value is determined by projecting the Gamillus intensity of each pixel on the polarity vector. The intensity of granzyme is multiplied by the cosine of the angle between the polarity vector and individual vector of the Gamillus pixel from the centre position of cells. The sum of the projected Gamillus intensities is normalized by the sum of all the Gamillus intensities in the cell.

Analysis of cell death following exogenous treatment with perforin and doxorubicin

The 1E7 cells were induced with at indicated concentration of doxycycline for 24 h before treatment with the agents. Recombinant perforin (abx652309; Abbexa) was diluted from 0.02 or 0.20 mg ml^{-1} in a buffer (20.0 mM HEPES, 150.0 mM NaCl, 2.5 mM $CaCl_2$, pH 7.4) and incubated with 1E7 cells at 37 °C for 30 min. Doxorubicin (S1208; Selleck Chemicals) was diluted from 0 to 2,000 nM in MCF10A cell culture media and incubated with 1E7 cells for 48 h before the measurement of cell death. PI (20 µg ml^{-1}, Sigma) was added to each cell for 10 min or Fixable Viability Dye 780 (1:1,000) was added to each cell for 30 min. Attune NxT flow cytometry (Thermo Fisher Scientific) was used for analysis.

CORA

CORA was performed as previously reported[56]. Briefly, glycoengineered cells were plated in a T75 culture flask with serum-free and phenol-red-free DMEM/F12-supplemented 20 ng ml^{-1} epidermal growth factor, 10 mg ml^{-1} insulin, 500 ng ml^{-1} hydrocortisone, 100 ng ml^{-1} cholera toxin and 1× penicillin/streptomycin. Then, 1 µg ml^{-1}

of doxycycline was incubated for 24 h before treatment with 80 μM peracetylated GalNAc-O-Bn. After 72 h, the media were aspirated, and loose cells and debris were removed by centrifugation. The supernatant was then filtered (Millipore Amicon Ultra 4, 10 kDa molecular weight cut-off). Glycosylated products were purified from a culture medium using Sep-Pak C18 cartridges (Waters), permethylated and analysed using electrospray ionization liquid chromatography with tandem mass spectrometry (LC-MS/MS, Q-Exactive MS Orbitrap). LC condition: xBridge CSH C18 3.5 μM, 4.6 × 150.0 mm^2 column; 0.1 ml min^{-1} flow rate; gradient going to 40.0% acetonitrile with 0.1% formic acid over 10 min, followed by a linear gradient to 90.0% acetonitrile + 0.1% formic acid at 50 min and a final 10 min wash with 100.0% acetonitrile + 0.1% formic acid. MS mass tolerance was 10 ppm, and MS2 fragmentation was performed using high-collision dissociation (18.3 eV). All the glycan structures were validated using MS/MS, and linkages were assigned on the basis of biochemical knowledge.

Fluorescence recovery after photobleaching

Fluorescence recovery after photobleaching experiments were performed by using a ZEISS i880 confocal microscope with ×63 1.4-numerical-aperture oil-immersion lens. Five pre-bleached images were taken and photobleaching was performed with a 488 nm laser for about 10 s to bleach a target area of 2.55 μm × 2.55 μm. Then, 10 μM recombinant human Gal-1 was incubated with 1E7 *GCNT1* OE cells for 10 min at 37 °C. Intensity profiles were corrected by normalizing to the time-course decay of the GFP signal in a non-bleached area and analysed by curve fitting to calculate the half-time of recovery ($T_{1/2}$) and mobile fraction using he MATLAB code available via the Janelia Advanced Imaging Center (https://www.mathworks.com/matlabcentral/fileexchange/47327-frap-zip).

Cell growth assay

The total DNA content of each cell line was quantified using QuantiFluor dsDNA System (no. E2671, Promega) following the manufacturer's protocol. Briefly, two replicates of each cell line were plated in 48-well cell culture plates (677180, Greiner) for each time point at an initial density of 5,000 cells cm^{-2}. At the indicated timepoints, the cells were lysed with 100 μl of Caron's Buffer (25 mM Tris-HCL, 0.4 M NaCl, 0.5% sodium dodecyl sulfate) for 10 min at 37 °C and stored at −80 °C. The cell lysates were centrifuged to remove the cell debris. The supernatants were diluted with QuantiFluor working solution in a 96-well plate with DNA standards. The fluorescence of the samples was measured with a microplate reader (Tecan).

SAIM

Supplementary Note 1 provides the descriptions of the SAIM optical setup, sample preparation, image acquisition and analysis, and have been described previously[22].

Preparation of recombinant proteins

Recombinant human galectins, GFP nanobody and StcE mucinases were produced in *E. coli* following standard protocols. Supplementary Notes 2–4 provide the complete descriptions.

Statistical methods, sample sizes, data collection and assumptions

The sample sizes were selected on the basis of standards in the field and not pre-determined using statistical methods. For statistical comparisons, data distributions were assumed to be normal. Normality was tested for conditions with approximately ten or more data points. Data collection and analyses were not performed blind to the conditions of the experiments. All the statistical analyses were performed using GraphPad Prism 8 software. All the experimental data are presented as mean ± s.d or as box-and-whisker plots with the first and third quartiles (boxes), median and range of data. Appropriate statistical tests were used to analyse the data, as described in the figure legends.

Reporting summary

Further information on research design is available in the Nature Portfolio Reporting Summary linked to this article.

Data availability

Raw data are available from the corresponding author upon request. Source data are provided with this paper.

Code availability

Packages for fitting the SAIM image sequences with the above model have been implemented in C++ and Julia and are available via GitHub at https://github.com/mjc449/SAIMscannerV3 and https://github.com/paszeklab/SAIMFitKit.jl.

References

49. Pan, H., Colville, M. J., Supekar, N. T., Azadi, P. & Paszek, M. J. Sequence-specific mucins for glycocalyx engineering. *ACS Synth. Biol.* **8**, 2315–2326 (2019).
50. Schönfeld, K. et al. Selective inhibition of tumor growth by clonal NK cells expressing an ErbB2/HER2-specific chimeric antigen receptor. *Mol. Ther.* **23**, 330–338 (2015).
51. Xiao, Q. et al. Size-dependent activation of CAR-T cells. *Sci. Immunol.* **7**, eabl3995 (2022).
52. Shurer, C. R. et al. Genetically encoded toolbox for glycocalyx engineering: tunable control of cell adhesion, survival, and cancer cell behaviors. *ACS Biomater. Sci. Eng.* **4**, 388–399 (2018).
53. Chitirala, P. et al. Studying the biology of cytotoxic T lymphocytes in vivo with a fluorescent granzyme B-mTFP knock-in mouse. *eLife* **9**, e58065 (2020).
54. Shinoda, H. et al. Acid-tolerant monomeric GFP from olindias FORMOSA. *Cell Chem. Biol.* **25**, 330–338.e7 (2018).
55. Bryceson, Y. et al. Functional analysis of human NK cells by flow cytometry. in *Natural Killer Cell Protocols* **612**, 335–352 Humana Press, (2010).
56. Wang, S.-S. et al. Efficient inhibition of O-glycan biosynthesis using the hexosamine analog Ac5GalNTGc. *Cell Chem. Biol.* **28**, 699–710.e5 (2021).

Acknowledgements

This investigation was supported by the National Science Foundation (NSF) grant 1752226 (M.J.P.), the Breast Cancer Coalition of Rochester predoctoral fellowship (S.P.) and the following National Institutes of Health (NIH) grants: CA276398 (M.J.P.), GM229133 (M.J.P.), CA210184 (M.J.P. and C.F.), CA193043 (M.J.P. and W.R.Z.), GM138692 (M.J.P.), GM137314 (M.J.P and M.D.), AI147362 (M.K.), T32AI007285 (C.J.S.) and CA273349 (S.N.). NGM138692 supported the glycoengineered cell-line development and glycocalyx material characterization. Work was performed at the Cornell Nanoscale Facility (NSF NNCI-2025233), Biotechnology Resource Center (RRID:SCR_021740) and Imaging Facility (RRID:SCR_021741) with NYSTEM (C029155) and NIH (S10OD018516) funding the ZEISS LSM880 instrument. The SAIM instrument development was supported by the Kavli Institute at Cornell for Nanoscale Science and project no. CA193043. We thank X. Su for providing the CD19 CAR cDNA and S. Malaker for helpful insights.

Author contributions

All authors contributed to the design of experiments, interpretation of results and preparation of the manuscript. Construction of plasmids, preparation of cell lines and execution of experiments were performed by S.P., M.J.C., J.H.P., C.R.S., A.S., E.J.S., C.J.S., L.-T.H., J.C.-H.K, M.C.G.

and J.S. M.J.C. built the SAIM microscope. C.J.S. and M.K. generated the CAR T cells. A.S. and S.N. conducted the CORA analysis. S.P. and M.J.P. wrote the manuscript with feedback from all authors.

Competing interests

Cornell's Center for Technology Licensing has submitted a patent related to the findings of this work with two authors (S.P. and M.J.P.) listed as the inventors (PCT/US2022/080937). All other authors declare no competing interests.

Additional information

Extended data is available for this paper at https://doi.org/10.1038/s41563-024-01808-0.

Supplementary information The online version contains supplementary material available at https://doi.org/10.1038/s41563-024-01808-0.

Correspondence and requests for materials should be addressed to Matthew J. Paszek.

Peer review information *Nature Materials* thanks Kamil Godula, Heinz Läubli and the other, anonymous, reviewer(s) for their contribution to the peer review of this work.

https://doi.org/10.1038/s41563-024-01808-0

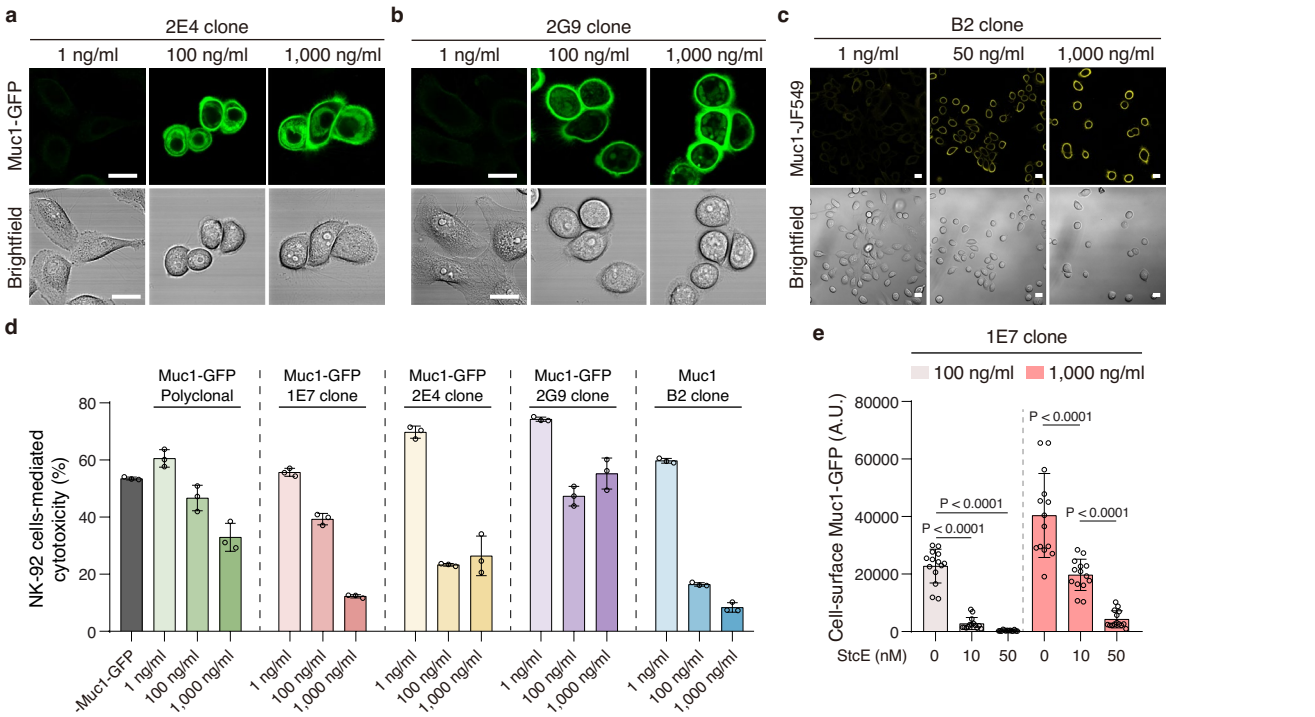

Extended Data Fig. 1 | Additional analysis of Muc1-mediated protection against NK cell cytotoxic function. a,b, Representative confocal and brightfield images of two clonally expanded MCF10A cell lines expressing Muc1-GFP with 42 tandem repeats (TRs) under the control of a tetracycline inducible promoter at the indicated doxycycline induction level. Scale bars, 10 µm. **c**, Representative confocal and brightfield images of Muc1-expresssing B2 clonal cells labelled with anti-Human Muc1 Janelia Fluor 549; the doxycycline induction level is indicated. Scale bars, 10 µm. **d**, NK-92 cell-mediated cytotoxicity against the polyclonal Muc1-GFP and three Muc1-GFP expressing clonal cell lines (1E7, 2E4, and 2G9) expressing MCF10A line from which the clonal lines were isolated, and a clonal MCF10A cell line expressing the Muc1 construct without the GFP reporter (B2 clone); the doxycycline induction levels are indicated. Results are the mean ± s.d of n =3 experimental replicates. NK cell to target cell ratio is 5:1. **e**. Mean fluorescence intensity of cell-surface Muc1-GFP in 1E7 cells treated with the indicated concentration of StcE mucinase; cell-surface Muc1-GFP probed with Alexa Fluor 647 conjugated GFP nanobody. Results are shown for induction of Muc1-GFP at 100 ng/ml and 1000 ng/ml doxycycline. Results are the mean ± s.d. of at least 14 cells from one representative of 3 independent experiments. Statistical analysis by one-way ANOVA with multiplicity-adjusted P values from Tukey's multiple comparisons test.

https://doi.org/10.1038/s41563-024-01808-0

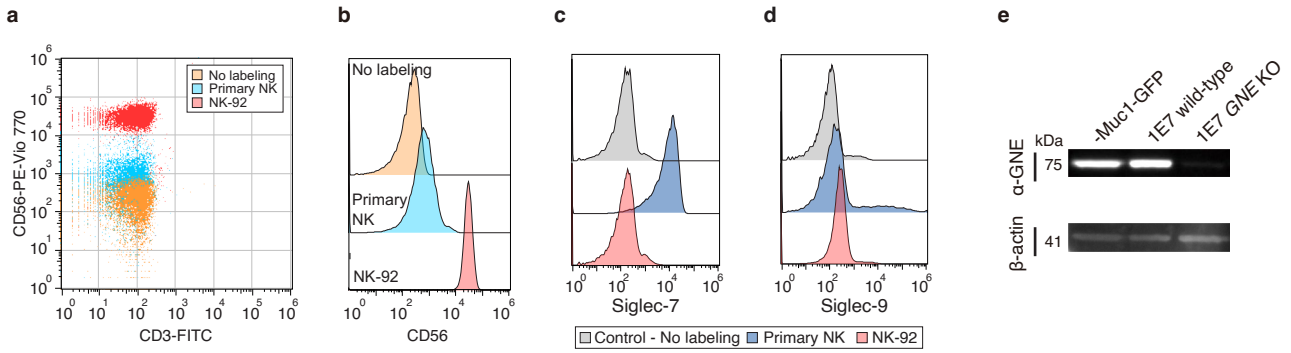

Extended Data Fig. 2 | Additional data supporting Siglec-independent protection by the mucin layer. a, b, Surface expression levels of CD3 (a) and CD56 (b) in NK-92 cells and primary NK cells analyzed by flow cytometry, validating isolation of CD56+/CD3- NK cells. **c, d**, Surface levels of Siglec-7 (c) and Siglec-9 (d) on NK-92 and primary human NK cells evaluated by flow cytometry, demonstrating minimal to no detectable levels of the receptors on NK-92. **e**, Western blot analysis confirming UDP-N-acetylglucosamine 2-epimerase (GNE) knockout (KO) in 1E7 cells to ablate sialylation. Flow cytometry data for primary NK cells are representative results for one of n =3 human blood donors.

https://doi.org/10.1038/s41563-024-01808-0

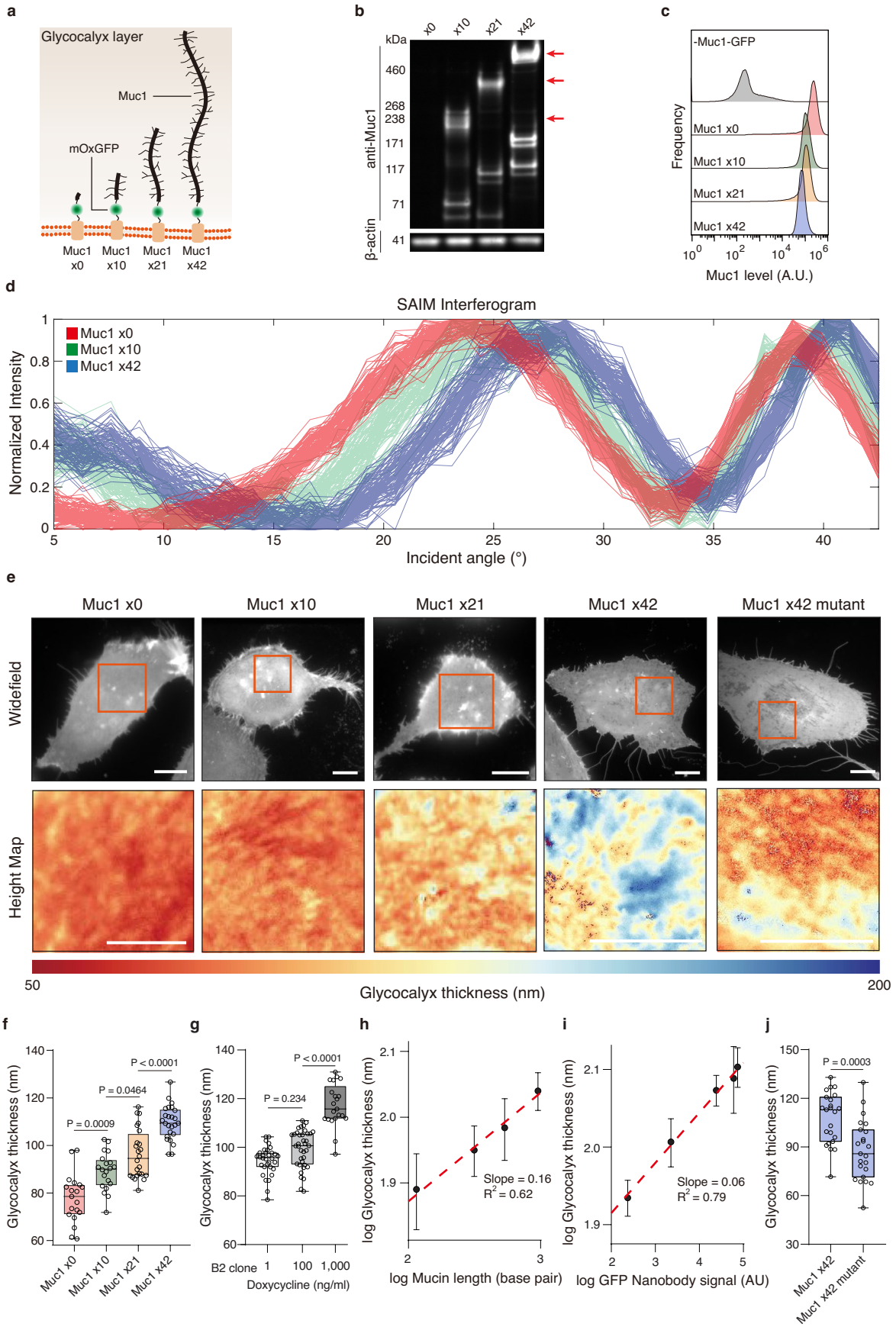

Extended Data Fig. 3 | See next page for caption.

https://doi.org/10.1038/s41563-024-01808-0

Extended Data Fig. 3 | Measurement of the nanoscale glycocalyx thickness with Ring Scanning Angle Interference Microscopy (Ring-SAIM). a, Muc1-GFP size standards with biopolymer domains comprised of 0, 10, 21, and 42 tandem repeats (TRs). **b**, Western blot analysis of Muc1-GFP constructs stably expressed in MCF10A epithelial cells; arrows indicate fully glycosylated Muc1 with 10, 21, or 42 TRs; the primary antibody reacts with the Muc1 TRs and does not probe the 0TR Muc1. **c**, Flow cytometry analysis of cell-surface Muc1-GFP probed with Alexa Fluor 647 conjugated GFP nanobody. **d**, Examples of the pixelwise SAIM interferograms for Muc1-GFP constructs labelled with Alexa Fluor 647 conjugated GFP nanobody. **e**, Representative widefield image and glycocalyx thickness map of live MCF10A epithelial cells expressing the indicated Muc1 constructs labeled with Alexa Fluor 647 conjugated GFP nanobody; the Muc1 x42 mutant construct is comprised of 42 TRs of the mutated Muc1 tandem repeat – PDARPAPGATAPPAHGVTAA – which has three of the five serine/threonine O-glycosylation sites mutated to alanine. Scale bars, 10 μm. **f, g**, Quantification of glycocalyx thickness in cells expressing the indicated Muc1 constructs (f) and the Muc1-expressing B2 clonal line induced at the indicated doxycycline levels (b). Boxes and whiskers show the first and third quartiles (boxes), median, and range of the data. Each condition includes a minimum of 19 cells from a representative experiment (n=3 independent experiments). Statistical analysis by one-way ANOVA with Tukey's post-hoc tests. **h**, Log of the mean glycocalyx thickness versus log of the mucin biopolymer length from (f); best-fit line to a power-law model with slope = 0.16 and R2= 0.62. **i**, Log of the mean glycocalyx thickness in 1E7 cells expressing Muc1-GFP at varying doxycycline induction levels versus the log of the mean GFP nanobody signal, a proportionate measure of Muc1 surface density; plotted data from Fig. 2f and Fig. 1d; best-fit line to a power-law model has slope = 0.06 and R2 = 0.79. **j**, Quantification of glycocalyx thickness in cells expressing the Muc1 x42 and the Muc1 x42 mutant construct. Boxes and whiskers show the first and third quartiles (boxes), median, and range of the data. Each condition includes a minimum of 23 cells from a representative experiment (n=3 independent experiments). Statistical analysis by two-tailed t tests. Unless otherwise indicated, doxycycline induction of mucin expression is at 1,000 ng/ml.

https://doi.org/10.1038/s41563-024-01808-0

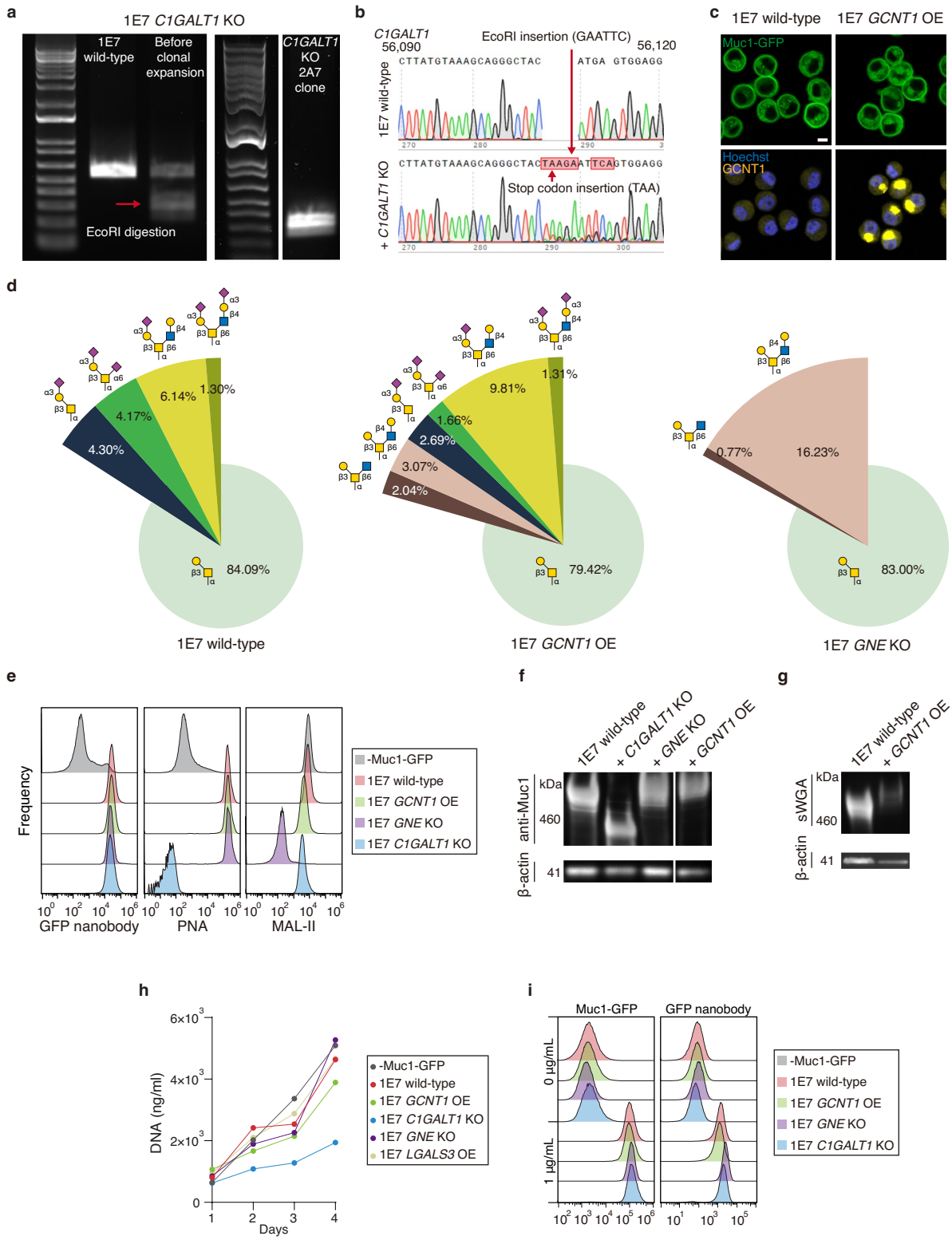

Extended Data Fig. 4 | See next page for caption.

https://doi.org/10.1038/s41563-024-01808-0

Extended Data Fig. 4 | Validation of glycoengineered cell lines. a, Agarose gel electrophoresis of PCR-amplified and EcoRI-digested segment of C1GALT1 showing successful homozygous knockout (KO) in 1E7 cells (See 2A7 sub-clone of 1E7); the homology directed repair (HDR) template for CRISPR/Cas9 mediated C1GALT1 KO introduces a unique EcoRI site. **b**, Sanger-sequencing results of a PCR-amplified segment of C1GALT1 with insertion of EcoRI restriction site (GAATTC) and stop codon (TAA) in the 1E7 C1GALT1 KO clone, verifying homozygous KO. (Top: 1E7; bottom: 1E7 C1GALT1 KO) **c**, Fluorescence images of Glucosaminyl (N-Acetyl) Transferase 1 (GCNT1) in wild-type and GCNT1 overexpressing (GCNT1 OE) 1E7 cells with Muc1-GFP expression induced at 1,000 ng/ml of doxycycline; GCNT1 is localized in the Golgi. **d**, Relative composition of Core O-glycans in wild-type, 1E7 GCNT1 OE, and 1E7 GNE KO cells measured with the Cellular O-glycome Reporter (CORA) method **e**, Flow cytometry analysis of wild-type and glycoengineered 1E7 cells. Results for the parental MCF10A epithelial cells that do not express Muc1-GFP (-Muc1-GFP) are included as a control. **f**, Western blot showing the relative size of Muc1 in the wild-type and glycoengineered 1E7 cells. **g**, sWGA lectin blot after extended SDS-PAGE run time showing increased molecular weight of Muc1-GFP in 1E7 GCNT1 OE cells compared to wild-type 1E7 cells. **h**, Rate of proliferation of wild-type and glycoengineered 1E7 cells. Results are the mean of 2 independent experiment replicates. **i**, Flow cytometry analysis of 1E7 cells and their glycoengineered progeny induced at 0 ng/ml and 1,000 ng/ml of doxycycline.

https://doi.org/10.1038/s41563-024-01808-0

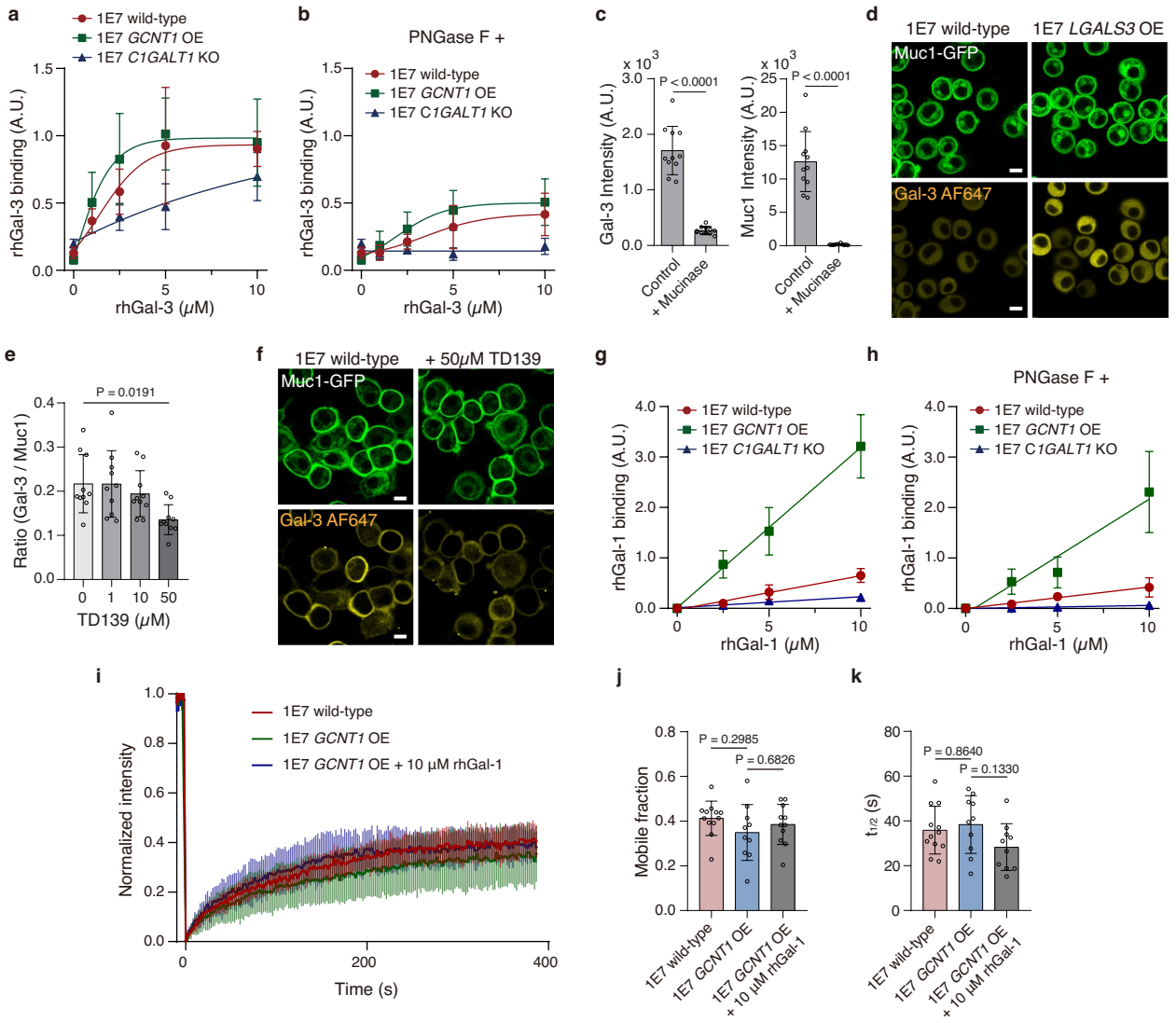

Extended Data Fig. 5 | Galectin interactions with Muc1 O-glycans. **a**, Quantification of recombinant human galectin-3 (rhGal-3) binding to wild-type, C1GALT1 knockout (KO), and GCNT1 overexpressing (OE) 1E7 cells; data normalized to the Muc1 signal intensity and presented as the mean and ± s.d. of 20 cells from one representative of n = 3 independent experiments. **b**, Same as in a, with 5,000 U/mL PNGase F treatment to selectively remove N-glycans prior to analysis. **c**, Quantification of endogenous cell-surface galectin-3 (Gal-3) and Muc1 before and after treatment with 200 nM StcE mucinase. Results are the mean ± s.d. of at least 11 cells from one representative of n = 3 independent experiments. Statistical analysis by two-tailed t tests. **d**, Representative confocal images of Muc1-GFP and immuno-labelled Gal-3 in wild-type and LGALS3 overexpressing (LGALS3 OE) 1E7 cells. Scale bars, 10 μm. **e**, Quantification of endogenous Gal-3 on the 1E7 cell surface following treatment with the indicated concentration of galectin inhibitor, TD139; data normalized to the Muc1 signal intensity and presented as the mean ± s.d. of 10 cells from one representative of n = 3 independent experiments. **f**, Representative confocal images of endogenous galectin-3 on the cell membrane in presence and absence of 50μM TD139. Scale bars, 10 μm. **g**, Quantification of recombinant human galectin-1 (rhGal-1) binding to wild-type and glycoengineered 1E7 cells; data normalized to the Muc1 signal intensity and presented as the mean ± s.d. of 20 cells from one representative of n = 3 independent experiments. **h**, Same as in g with 5,000 U/mL PNGase F treatment to selectively remove N-glycans prior to analysis. **i**, FRAP analysis of Muc1-GFP in wild-type and 1E7 GCNT1 OE cells treated with control buffer, as well as 1E7 GCNT1 OE cells treated with 10 μM rhGal-1. Results are the mean ± s.d. of intensity profiles of n= 11, 10, 9 cells, respectively. **j, k**, Quantification of mobile fraction (j) and half recovery time (k) from (i). In all experiments, Muc1-GFP expression was induced with 1,000 ng/ml of doxycycline. Unless otherwise indicated, statistical analysis by one-way ANOVA with multiplicity-adjusted P values from Tukey's multiple comparisons test.

https://doi.org/10.1038/s41563-024-01808-0

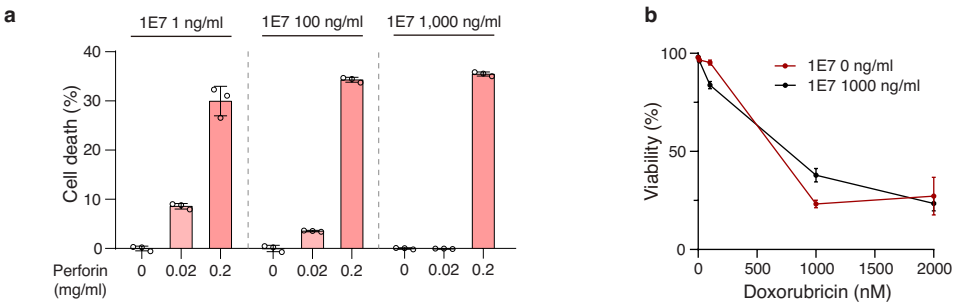

Extended Data Fig. 6 | Apoptosis is not inhibited by Muc1-GFP expression. **a**, Quantification of 1E7 cell death resulting from treatment with the indicated concentrations of recombinant perforin for 30 minutes; Muc1-GFP expression induced at 1, 100, 1,000 ng/ml doxycycline. Results are the mean ± s.d. of n = 3 technical replicates for one representative of three independent experiments. **b**, Quantification of cell viability (%) of uninduced (0 ng/ml) and doxycycline-induced (1,000 ng/ml) 1E7 cells following treatment with indicated concentration of doxorubicin for 48 hours. Results are the mean ± s.d. of n = 3 technical replicates.

https://doi.org/10.1038/s41563-024-01808-0

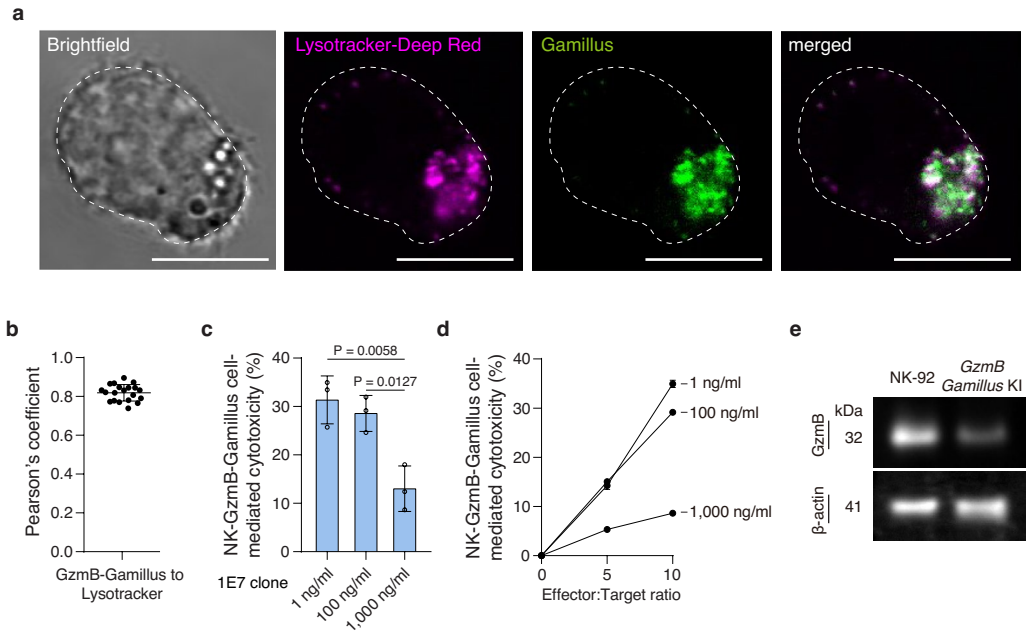

Extended Data Fig. 7 | Validation of endogenous labeling of Granzyme B (GzmB) in NK-92 cells. Using CRISPR/Cas9 and an appropriate homology directed repair template, the gene sequence for a flexible GGSGGSGGS linker and the pH-tolerant green fluorescent protein, Gamillus, was inserted immediately before the endogenous GZMB stop codon in NK-92 cells. **a**, Representative brightfield and fluorescence images of NK-92 GzmB-Gamillus cells stained with Lysotracker Deep Red. Scale bar, 10µm. **b**, Pearson's coefficients of correlation between GzmB-Gamillus and Lysotracker. Results are the mean ± s.d. of 20 cells. **c, d**, NK-92 GzmB-Gamillus mediated cytotoxicity against 1E7 with Muc1-GFP expression induced at the indicated doxycycline concentration. Results are the mean ± s.d. of n =3 independent experimental replicates. NK cell to target cell ratio is 10:1. Statistical analysis by one-way ANOVA with multiplicity-adjusted P values from Tukey's multiple comparisons test. **e**, Western blot showing the relative expression level of Granzyme B (GzmB) in the NK-92 cells and NK-92 GzmB-Gamillus knock-in (KI) cells. Note that the acid-labile linker between GzmB and Gamillus is expected to undergo cleavage in the low pH of lysosomes and cytolytic granules.

https://doi.org/10.1038/s41563-024-01808-0

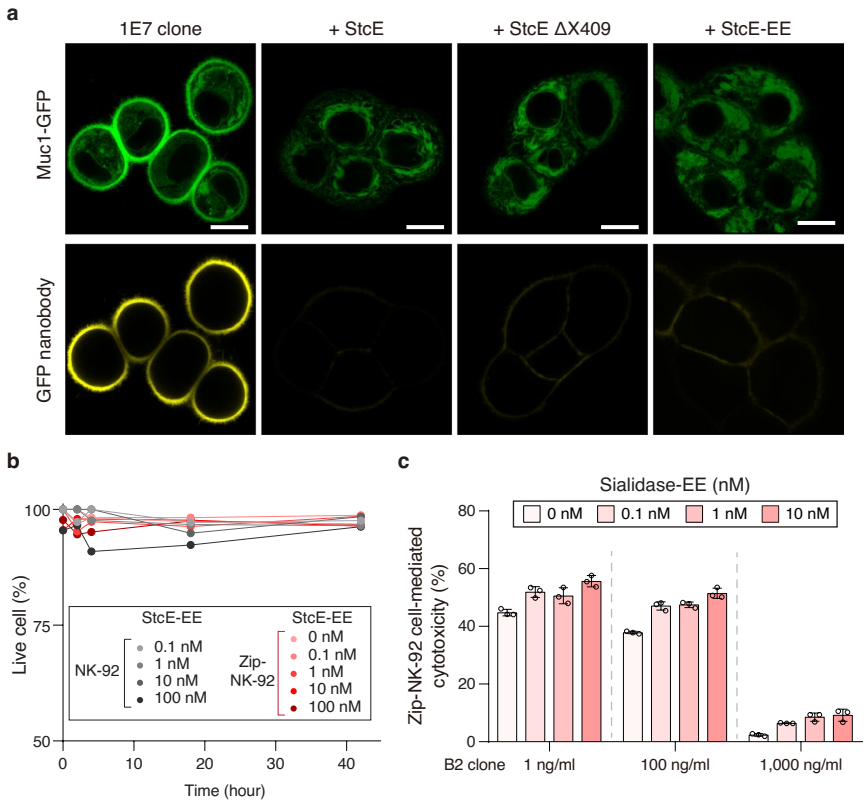

Extended Data Fig. 8 | Supporting characterization for StcE NK-92 and Zip-NK-92 cells. a, Representative confocal images of Muc1-GFP on 1E7 cells treated with control buffer or 100 nM StcE, StcE ΔX409, StcE ΔX409 fused to the EE leucine zipper (StcE-EE); Alexa Fluor 647 conjugated GFP nanobody is used to probe cell-surface Muc1-GFP constructs. Scale bar, 10 μm. **b**, Viability of NK-92 and Zip-NK-92 after treatment with indicated concentration of StcE-EE. Propidium iodide (20 μg/ml) was used to detect dead cell population by flow cytometry. **c**, Cytotoxicity mediated by Zip-NK-92 cells coupled with the indicated concentration of Sialidase-EE zipper fusion protein (Sialidase-EE) against B2 cells at the indicated doxycycline induction level; NK cell to target cell ratio is 5:1. Results are the mean ± s.d. of n = 3 technical replicates for each doxycycline concentration.

nature portfolio

Corresponding author(s): Matthew J. Paszek

Last updated by author(s): Aug 10, 2023

Reporting Summary

Nature Portfolio wishes to improve the reproducibility of the work that we publish. This form provides structure for consistency and transparency in reporting. For further information on Nature Portfolio policies, see our Editorial Policies and the Editorial Policy Checklist.

Statistics

For all statistical analyses, confirm that the following items are present in the figure legend, table legend, main text, or Methods section.

n/a	Confirmed	
☐	☒	The exact sample size (*n*) for each experimental group/condition, given as a discrete number and unit of measurement
☐	☒	A statement on whether measurements were taken from distinct samples or whether the same sample was measured repeatedly
☐	☒	The statistical test(s) used AND whether they are one- or two-sided *Only common tests should be described solely by name; describe more complex techniques in the Methods section.*
☒	☐	A description of all covariates tested
☐	☒	A description of any assumptions or corrections, such as tests of normality and adjustment for multiple comparisons
☐	☒	A full description of the statistical parameters including central tendency (e.g. means) or other basic estimates (e.g. regression coefficient) AND variation (e.g. standard deviation) or associated estimates of uncertainty (e.g. confidence intervals)
☐	☒	For null hypothesis testing, the test statistic (e.g. *F*, *t*, *r*) with confidence intervals, effect sizes, degrees of freedom and *P* value noted *Give P values as exact values whenever suitable.*
☒	☐	For Bayesian analysis, information on the choice of priors and Markov chain Monte Carlo settings
☒	☐	For hierarchical and complex designs, identification of the appropriate level for tests and full reporting of outcomes
☐	☒	Estimates of effect sizes (e.g. Cohen's *d*, Pearson's *r*), indicating how they were calculated

Our web collection on statistics for biologists contains articles on many of the points above.

Software and code

Policy information about availability of computer code

Data collection	Attune NxT flow cytometry (Thermo Fisher) and MA900 Cell Sorter (Sony) were used for flow cytometry data acquisition. Q-Exactive MS Orbitrap (Thermo Fisher) was used for glycan structure analysis. A infinite M1000Pro plate reader (Tecan) was used for absorbance and fluorescence detection in a 96 well plates. NanoDrop™ OneC Spectrophotometer (Thermo Fisher) was used to characterize proteins and DNAs. ChemiDoc MP Imaging System (Bio-Rad) was used for gel scanning. Fluorescence images of cells were acquired using Zeiss i880 confocal microscope, LSM 800 confocal microscope (Zeiss), and custom circle-scanning microscope with a Zyla 4.2 sCMOS (Andor) and an iXon 888 EMCCD (Andor), controlled with Micro-Manager.
Data analysis	Microsoft Excel for Microsoft 365 MSO (Version 2307), GraphPad Prism (v8), MATLAB R2019a, ImageJ (v1.53s), Julia (v1.3.0) and Visual Studio 2017 were used for data analysis and curve-fitting. FlowJo (v10) was used for flow cytometry data analysis.

For manuscripts utilizing custom algorithms or software that are central to the research but not yet described in published literature, software must be made available to editors and reviewers. We strongly encourage code deposition in a community repository (e.g. GitHub). See the Nature Portfolio guidelines for submitting code & software for further information.

Data

Policy information about availability of data

All manuscripts must include a data availability statement. This statement should provide the following information, where applicable:

- Accession codes, unique identifiers, or web links for publicly available datasets
- A description of any restrictions on data availability
- For clinical datasets or third party data, please ensure that the statement adheres to our policy

All raw data for figures shown in this manuscript are provided as Source data files. Any unique biological materials presented in the manuscript may be available from the authors upon reasonable request and through a materials transfer agreement.

Research involving human participants, their data, or biological material

Policy information about studies with human participants or human data. See also policy information about sex, gender (identity/presentation), and sexual orientation and race, ethnicity and racism.

Reporting on sex and gender	N/A - Our studies are not classified as human subject research according to the definitions of the National Institutes of Health; All human biospecimens (e.g. blood for immune cell isolation) were obtained as de-identified products
Reporting on race, ethnicity, or other socially relevant groupings	N/A
Population characteristics	N/A
Recruitment	N/A
Ethics oversight	N/A

Note that full information on the approval of the study protocol must also be provided in the manuscript.

Field-specific reporting

Please select the one below that is the best fit for your research. If you are not sure, read the appropriate sections before making your selection.

☒ Life sciences ☐ Behavioural & social sciences ☐ Ecological, evolutionary & environmental sciences

For a reference copy of the document with all sections, see nature.com/documents/nr-reporting-summary-flat.pdf

Life sciences study design

All studies must disclose on these points even when the disclosure is negative.

Sample size	Sample sizes were based on typical sizes in the field; statistical methods were not used to pre-determine sample sizes.
Data exclusions	N/A
Replication	Multiple biological and/or experimental replicates were conducted as noted in the figure legends.
Randomization	Cells were selected at random for all single-cell analyses.
Blinding	Data collection and analyses were not performed blind to the conditions of the experiments.

Reporting for specific materials, systems and methods

We require information from authors about some types of materials, experimental systems and methods used in many studies. Here, indicate whether each material, system or method listed is relevant to your study. If you are not sure if a list item applies to your research, read the appropriate section before selecting a response.

Materials & experimental systems

n/a	Involved in the study
☐	☒ Antibodies
☐	☒ Eukaryotic cell lines
☒	☐ Palaeontology and archaeology
☐	☒ Animals and other organisms
☒	☐ Clinical data
☒	☐ Dual use research of concern
☒	☐ Plants

Methods

n/a	Involved in the study
☒	☐ ChIP-seq
☐	☒ Flow cytometry
☒	☐ MRI-based neuroimaging

Antibodies

Antibodies used

anti-Human Muc1 Clone HMPV (555925, BD Biosciences)
anti-Human Muc1 Janelia Fluor 549 (NBP-2-47883JF549, Novus Biologicals)
Recombinant anti-GNE antibody (ab189927, Abcam)
anti-GCNT1 antibody (ab102665, Abcam)
anti-Galectin-3 (sc-19280, Santa Cruz Biotechnology)
mouse anti-β-Actin Clone C4 (sc-47778, Santa Cruz Biotechnology)
anti-ErbB2/HER2 Clone 3B5 (ab16901, Abcam)
APC conjugated anti-Human perforin Clone dG9 (30811, BioLegend)
Anti-6X His-tag antibody (ab9108, Abcam)
anti-CD19 antibody (ab134114, Abcam)
APC conjugated anti-human CD328 (Siglec-7; #339205; BioLegend)
anti-human Siglec-9 (MAB1139-SP; R&D systems)
PE-Vio770 conjugated anti-human CD56 (#130-113-870; Miltenyi Biotec)
FITC conjugated anti-human CD3 (#130-113-690; Miltenyi Biotec)
goat anti-mouse IgG DyLight 800 4x PEG conjugate (SA535521, Invitrogen)
goat anti-mouse IgG DyLight 680 conjugate (35518, Invitrogen)
goat anti-rabbit IgG Alexa Fluor 647 conjugate (A21245, Thermo Fisher Scientific)
goat anti-mouse Alexa Fluor 647 conjugate (A28181, Invitrogen)
rabbit anti-goat IgG Alexa Fluor 647 conjugate (A21446, Invitrogen)
CF640R-conjugated PNA (#29063, Biotium)
biotin-conjugated MAL-II (B-1265-1, Vector Laboratories)
biotin-conjugated sWGA (B-1025S-5, Vector laboratories)
NeutrAvidin Protein DyLight 800 conjugate (22853, Thermo Fisher Scientific)
NeutrAvidin Protein DyLight 650 conjugate (84607, Thermo Fisher Scientific)
FluoTag-X2 anti-ALFA conjugated with Alexa Fluor 647 (#N1502, NanoTag Biotechnologies)

Validation

All antibodies were obtained from commercial sources which provided authentication sheets. When possible, antibodies were additionally validated by confirming correct sub-cellular localization in immunolabeled cells and reactivity with proteins of the expected molecular weight via SDS-PAGE.

Eukaryotic cell lines

Policy information about cell lines and Sex and Gender in Research

Cell line source(s)

MCF10A, ZR-75-1, NK-92, SKOV3, Capan-2, KPL-1, SKBR3, and T47D were obtained from the American Tissue Culture Collection (ATCC). HEK293T were a gift of Valerie Weaver.

Authentication

With the exception of HEK293T, all cell lines were obtained as authenticated products from ATCC. HEK293T were used exclusively for lentiviral production and validated to produce functional viral particles.

Mycoplasma contamination

All cell lines were regularly tested and confirmed negative for mycoplasma infection (ABM Mycoplasma PCR Detection Kit).

Commonly misidentified lines
(See ICLAC register)

No commonly misidentified cells were used in this study.

Animals and other research organisms

Policy information about studies involving animals; ARRIVE guidelines recommended for reporting animal research, and Sex and Gender in Research

Laboratory animals

N/A

Wild animals

N/A

Reporting on sex

N/A

Field-collected samples	N/A
Ethics oversight	Blood collection for cell isolation from donor horses was approved by the Cornell IACUC

Note that full information on the approval of the study protocol must also be provided in the manuscript.

Flow Cytometry

Plots

Confirm that:

☒ The axis labels state the marker and fluorochrome used (e.g. CD4-FITC).

☒ The axis scales are clearly visible. Include numbers along axes only for bottom left plot of group (a 'group' is an analysis of identical markers).

☒ All plots are contour plots with outliers or pseudocolor plots.

☒ A numerical value for number of cells or percentage (with statistics) is provided.

Methodology

Sample preparation	Sample preparation is described in the methods
Instrument	Attune NxT flow cytometry (Thermo Fisher) and MA900 Cell Sorter (Sony)
Software	The FlowJo V10 software package was used for data analysis
Cell population abundance	The samples were more than 95% pure as determined by post-sort flow-cytometry analysis
Gating strategy	Examples and descriptions for all gating strategies are in the Supplementary Information. FSC-A/SSC-A plot was used to gate for the starting cell population. Singlets were selected with SSC-H/SSC-A plots. For example, for Muc1 staining in ZR-75-1 cells, the cells were gated based on cell-surface Muc1 expression, followed by normal gating on area FSC-A/SSC-A followed by single cell gating with FSC-A/FSC-H.

☒ Tick this box to confirm that a figure exemplifying the gating strategy is provided in the Supplementary Information.